J. Fluid Mech. (1995), *vol.* 292, *pp.* 1–38

Passive scalar dispersion and mixing in a turbulent jet

By CHENNING TONG AND Z. WARHAFT

Sibley School of Mechanical and Aerospace Engineering, Cornell University, Ithaca, NY 14853, USA

(Received 30 August 1994 and in revised form 12 December 1994)

The dispersion and mixing of passive scalar (temperature) fluctuations is studied in a turbulent jet. The temperature fluctuations were produced by heated fine wire rings placed axisymmetrically in the flow. Typically the ring diameters were of the same order as the jet, D_j, and they were placed in the self-similar region. However, other initial conditions were studied, including a very small diameter ring used to approximate a point source. Using a single ring to study dispersion (which is analogous to placing a line source in a planar flow such as grid turbulence), it was found that the intense local thermal field close to the ring disperses and fills the whole jet in approximately 1.5 eddy turnover times. Thereafter the thermal field evolves in the same way as for the traditional heated jet experiments. Two heated rings were used to study the mixing of two independently introduced scalar fields. Here an inference method (invoking the principle of superposition) was used to determine the evolution of the cross-correlation coefficient, ρ, and the segregation parameter, α, as well as the coherence and co-spectrum. While initially strongly dependent on ring locations and spacing, ρ and α reached asymptotic values of 1 and 0.04, respectively, also in about 1.5 eddy turnover times. These results are contrasted with mixing and dispersion in grid turbulence where the evolution is slower. Measurements in the far field of the jet (where $\rho = 1$) of the square of the scalar derivative conditioned on the scalar fluctuation itself, as well as other conditional statistics, showed strong dependence on the measurement location, as well as the direction in which the derivative was determined. The cross-correlation between the square of the scalar derivative and the signal showed a clear Reynolds-number trend, decreasing as the jet Reynolds number was varied from 2800 to 18000. The far-field measurements, using the heated rings, were corroborated by new heated jet experiments.

1. Introduction

Scalar contaminants such as pollutants, chemical reactants, or temperature inhomogeneities, are often introduced into a background flow (be it the atmosphere, ocean or a laboratory flow) approximately at a point, or at least at a scale significantly smaller than that of the surrounding turbulence. Chimneys and fuel injectors are typical examples. The scalar is then dispersed by molecular and turbulent diffusion such that its scale increases, the inhomogeneities decrease, and the scalar concentration dilutes. If chemical reaction occurs then two scalars are involved, and these must be mixed by the turbulence so that there is a transfer of matter or heat between the two species down to molecular scales. Thus dispersion and mixing are intimately connected, the latter accentuating the interaction of two or more distinct species. One of these may be the surroundings themselves, but often two contaminants, A and B, are mixed in a

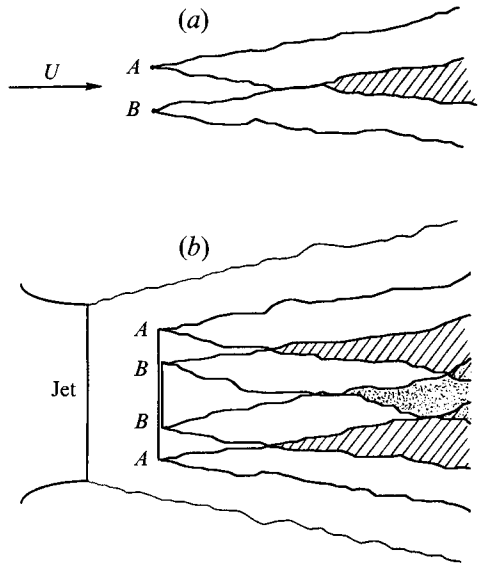

FIGURE 1. (*a*) The instantaneous thermal (or concentration) fields downstream from two line or point sources, *A* and *B*. Mixing occurs when the two plumes have dispersed so they begin to overlap (hatched region). This situation, for line sources in grid turbulence, was studied by Warhaft (1984). Here we study the analogous situation for a jet, using two fine wire heated rings as sources, shown (side view) in (*b*). Note that the axial symmetry allows for the overlap (and hence mixing) of one side of a ring with the other. This is shown as a dotted region. We are concerned however with the mixing from two distinct sources, thus we are interested in the hatched region.

third medium (such as the atmosphere). It is this problem that we will be particularly concerned with here.

While the connection between mixing and dispersion has been long recognized, particularly in models using particle dispersion techniques (Taylor 1921; Batchelor 1952; Durbin 1980; Hunt 1985), there has been relatively little attempt to relate them from an experimental point of view. Thus there are numerous experiments that focus on dispersion in various types of flows such as isotropic turbulence (Uberoi & Corrsin 1953; Townsend 1954; Warhaft 1984; Stapountzis *et al.* 1986; Nakamura, Sakai & Miyata 1987), homogeneous turbulence (Stapountzis & Britter 1989; Karnick & Tavoularis 1989), inhomogeneous turbulence without shear (Veeravalli & Warhaft 1990) and in inhomogeneous shear flows (Paranthoen *et al.* 1988; Fackrell & Robins 1982). Typically a line or point source (of heat or a chemical constituent) is introduced into the flow and the spreading of the mean and variance profiles is studied. Mixing experiments, on the other hand, are usually done by introducing the scalars throughout large regions of the flow and the mixing at their interface is studied. Typical examples are the shear layer experiments of Briedenthal (1981), where species *A* is introduced throughout one side of the mixing layer and species *B* throughout the other, or the numerous concentration and heated jet experiments where mixing of the jet interface with the surroundings is studied (Dowling & Dimotakis 1990, and references therein).

A combination of dispersion and mixing is shown in figure 1. Two species *A* and *B* are introduced into a turbulent flow. As they disperse the two plumes will come into contact and the scalars will mix. The mixing process is described in terms of the correlation coefficient $\rho(\equiv \langle c_A c_B \rangle / (\langle c_A^2 \rangle^{1/2} \langle c_B^2 \rangle^{1/2}))$. Here c_A and c_B are the fluctuations of the species concentration about the mean ($\langle C_A \rangle$ and $\langle C_B \rangle$) of the two respective scalars, and the angle brackets represent averaging (in the experiments to be

reported here, it is time averaging at a particular location in space). When, for the situation shown in figure 1, the two scalars are completely mixed with each other, $\rho = 1$, i.e. the scalars are perfectly correlated. Note that complete mixing means that the cross-correlation of unity must apply for all scales, i.e. the coherence (as a function of wave number or frequency) must be unity.

Another related way of describing the mixing process is in terms of the segregation parameter, $\alpha(\equiv \langle c_A c_B\rangle/(\langle C_A\rangle\langle C_B\rangle))$. This parameter, introduced by Danckwerts (1952), arises when considering the depletion rate of the reactants. Thus if we consider the unidirectional reaction between two initially unpremixed reactants, A and B (see for example Komori *et al.* 1991), the rate of change of the mean concentration of A is given by

$$\frac{\partial\langle C_A\rangle}{\partial t}+U_i\frac{\partial\langle C_A\rangle}{\partial x_i}=\frac{\partial[\kappa(\partial\langle C_A\rangle/\partial x_i)-\langle u_i c_A\rangle]}{\partial x_i}-k[\langle C_A\rangle\langle C_B\rangle+\langle c_A c_B\rangle], \quad (1)$$

where $C_A \equiv \langle C_A\rangle + c_A$ is the instantaneous concentration of A, κ and k are the molecular diffusivity and the chemical reaction rate constant respectively, and U_i and u_i are the mean and fluctuating velocities in the x_i direction. A similar equation can be written for $\langle C_B\rangle$. The second term on the right-hand side of (1) can be written in the form

$$-k\langle C_A\rangle\langle C_B\rangle[1+\alpha],$$

where α, the segregation parameter, has been defined above. If $\alpha = -1$ there is no molecular mixing since $C_A C_B = 0$. Clearly both the sign and magnitude of α play a vital role in the reaction, yet, as Komori *et al.* (1991) point out, it has been poorly documented. (Some workers have even set α equal to zero, thereby possibly accruing large error in their reaction rate calculations.) Note that while the sign of α is determined by the cross-correlation, its magnitude depends on the relative intensity of the fluctuations, $\langle c^2\rangle^{1/2}/\langle C\rangle$, and this varies from flow to flow.

In the work to follow, we will determine both ρ and α by a method of inference (Warhaft 1981, 1984). Here a single scalar (temperature) is introduced into the flow at two separate locations in a manner similar to figure 1. If the velocity field is statistically stationary, the scalar is passive, and the line source from which it is introduced is sufficiently small so that it does not affect the flow dynamics, then ρ or α can be determined by first operating source A, thereby allowing the mean and variance, T_A and $\langle\theta_A^2\rangle$, to be measured at a particular downstream location, then operating source B and measuring T_B and $\langle\theta_B^2\rangle$. Finally both sources are operated together and $T_A + T_B$ and $\langle(\theta_A+\theta_B)^2\rangle = \langle\theta_A^2\rangle+\langle\theta_B^2\rangle+2\langle\theta_A\theta_B\rangle$ are measured at the same location. Since $\langle\theta_A^2\rangle$ and $\langle\theta_B^2\rangle$ have already been measured, the covariance term, $\langle\theta_A\theta_B\rangle$, and thus ρ and α can be determined from this final measurement. The method has been used previously for distributed and line sources in grid turbulence (Warhaft 1981 and 1984 respectively), and has been shown by Sirivat & Warhaft (1982) to yield the same results as measurements using two different scalars (helium and temperature). Here we will use it for the study of mixing in a jet by placing two concentric fine heated wire rings downstream from the origin, as sketched in figure 1(*b*).

Apart from ρ and α, there are other important parameters in the mixing process. For example the smearing of the small-scale scalar fluctuations by molecular effects is described by the 'scalar dissipation' term $\epsilon_\theta \equiv \overline{\kappa(\partial\theta/\partial x_j)(\partial\theta/\partial x_j)}$. (Here we are using temperature fluctuations, θ, but the same discussion applies for species A or B.) It is of particular interest to know how ϵ_θ is conditioned by the value of the temperature fluctuations themselves, since the rate equation for the probability density function (p.d.f.) of a scalar explicitly contains the conditional dissipation as well as other

conditional terms (Pope 1985; Sahay & O'Brien 1993). We will determine these parameters and describe the relevant theory in the work to follow.

We have chosen a jet for our study of dispersion and mixing for a number of reasons. First, it is a basic and well-documented flow and, as mentioned above, there have been a number of experiments in which pure mixing (with the surrounding ambient air) has been studied. Thus we have reference conditions with which we can compare our results. Secondly, the jet has shear and inhomogeneity, characteristics that are invariably present in both industrial and atmospheric flows. In our previous experiments we studied mixing and dispersion in grid-generated turbulence, a flow which is homogeneous and without shear. Paradoxically there are some aspects of the more complex shear flows that make their study easier. We will show that the shear enhances the rate of mixing allowing clear asymptotic values to be measured. On the other hand grid turbulence evolves slowly and the asymptotic values of parameters such as α, ρ and $(\langle\theta^2\rangle)^{1/2}/T$ (the relative scalar intensity) are difficult to determine. Finally, the theoretical and computational work of Kerstein (1992) has provided impetus for this study. In the final section of his paper, Kerstein specifically addresses the problem of two-source mixing in a jet, and it seemed that the interference method was well suited to examine his predictions.

As mentioned above, we introduce the scalar field into the jet by means of two fine heated rings placed concentrically downstream of the jet exit (figure 1*b* and §2). (On most occasions the rings were in the same plane, but for some experiments one was shifted longitudinally with respect to the other.) In preliminary experiments (Warhaft 1992) it was found that the fine rings reduced the turbulence intensity of the jet when placed close to the jet exit (closer than at $x/D_j \sim 3$ where D_j is the jet diameter). Subsequently it was shown (Tong & Warhaft 1994*a*) that the rings slightly modify the mean velocity profile and this results in an inhibition of the vortex pairing mechanism, thereby suppressing the fluctuation intensity. However, if the rings were placed further downstream they had no measurable effect on the velocity field. Thus for most of the work to be reported here they will be placed at $x/D_j = 9$, just after the onset of the fully developed self-similar region of the jet. However, we will show that even if placed very close to the jet origin, the nature of the mixing and dispersion process does not appear to be significantly altered due to the rings effect on the velocity field.

The rings, whose diameters were generally of the order of that of the jet itself (although their diameters were varied over a relatively wide range) are analogous to line sources in grid turbulence. A further possible dispersion experiment is to place a point source along the jet axis. This is rather difficult to do because of the power required to heat the source, but an approximate point source was achieved by placing a very small ring along the jet centreline. Finally, some experiments were conducted using a heated jet and a combination of a heated jet and a ring.

The outline of the paper is as follows. After describing the apparatus in §2, we begin the results section by documenting the velocity field (§3.1). We then discuss the dispersion and mixing experiments by dividing the development of the thermal field into two stages: the near and the far field. In the near field the thermal fields from the rings disperse and then mix with each other as the thermal wakes grow wider (§§3.2 and 3.3). We will show that here the cross-correlation is initially negative and then builds up towards a value of $+1$ as the two thermal fields become completely mixed with each other. We define the near field as that region when $\rho < 1$. After $\rho \sim 1$, we will show that the evolution of the thermal field is independent of its initial conditions and that it behaves in the same way as the traditional heated jet experiments, i.e. the mixing is exclusively with the ambient air, and not between the fields from the line sources

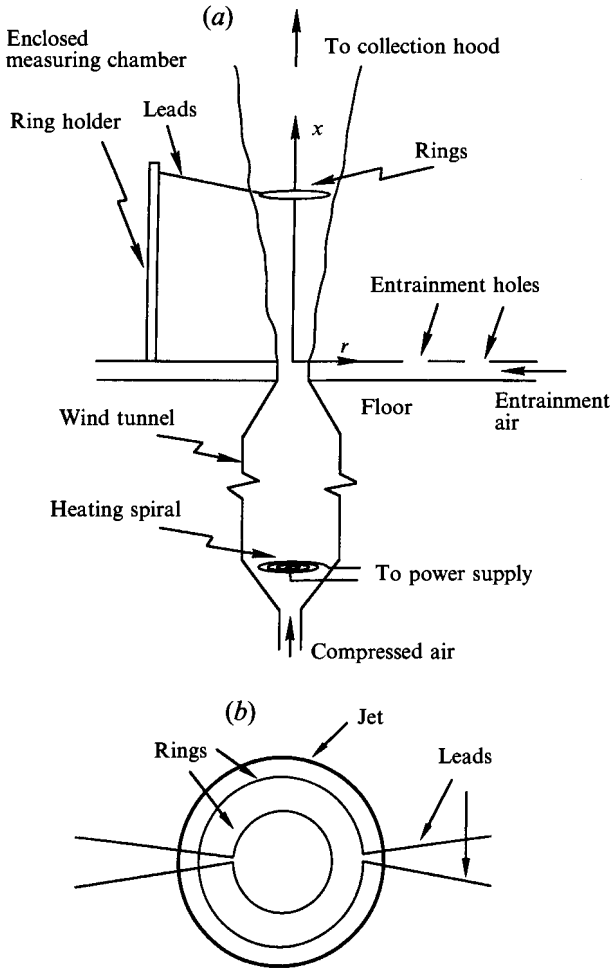

FIGURE 2. A sketch (not to scale) of the apparatus showing the two different methods of generating the thermal field. (*a*) Side view, only one ring is shown. (*b*) Plan view.

themselves. For both the near and far field we will document the downstream and lateral evolution of the mean, variance, and the relative intensity of the fluctuations. In the near field (§3.3) we will particularly be concerned with the covariance statistics between the two scalars (ρ, α, coherence, co-spectrum, etc.) while in the far field (§3.4) we will study p.d.f.'s and conditional statistics.

In concept the present work is an extension of Warhaft (1984) to a shear flow. However, here we examine aspects (particularly p.d.f.'s and conditional statistics) not studied in that previous work. Preliminary results of the present study appeared in Warhaft (1992). The effects of the rings on the velocity field are described in Tong *et al.* (1994*a*).

2. Apparatus

The air jet was originally constructed for velocity measurements in the region $30 \leqslant x/D_j \leqslant 150$, where D_j is the jet diameter (Panchapakesan & Lumley 1993). Here our measurements will be confined to the initial and the early part of the self-similar region, $0 \leqslant x/D_j \leqslant 40$. The jet issued vertically from the floor into a closed room of

dimensions $4.25 \times 4.25 \times 3.75$ m (figure 2). The air for the jet was supplied through a small wind tunnel of 10 cm diameter, by an air compressor. The jet flowed upwards into a collection hood on the ceiling (about 250 diameters downstream for the 15 mm jet in the present experiment). In order to match the flow rate through the hood, ambient air was entrained through the holes on the floor. This arrangement ensured minimum disturbance to the flow. Further details of the jet facility can be found in Panchapakesan & Lumley (1993).

As explained in the introduction, the thermal fields were formed by two different methods: by placing fine wire rings in the jet, and by the traditional way of heating the whole jet. The heated rings (which were self-supporting since the leads were copper coated (Tong & Warhaft 1994*a*)), were made from nichrome wire of 0.254 mm diameter, and were placed concentrically in the jet (mostly at $x/D_j = 9$) to study thermal dispersion and mixing from localized sources (figures 1*b* and 2). For most of these measurements, a 30 mm nozzle was used. The Reynolds number of the ring wire, when cold, was 95. When the rings were heated their Reynolds number was considerably reduced since the viscosity of the air surrounding the ring increased. The effects of the rings on the velocity field has been reported in Tong & Warhaft (1994*a*), where it was found that if the rings were placed at $x/D_j > 3$, their effects on the flow were negligible for ring wire Reynolds number varying from 30 to 120. In order to produce the temperature fluctuations, approximately 10 W of electrical power was applied to the rings. We also attempted to study thermal dispersion from a point source by placing a very small ring of diameter 2 mm on the jet centreline, at $x/D_j = 9$. Clearly this is not a ideal point source (the Kolmogorov scale in the jet was order of 0.1 mm), but smaller rings did not allow for enough power to provide sufficiently high temperature fluctuations for the measurements. We will show below that although only approximating a point source, the small ring gave very satisfactory results in the turbulent convective and diffusive regimes. For the heated jet experiment, a spiral of resistance ribbon was placed at the beginning of the wind tunnel as the heating element (figure 2). Because of the way the air was heated, the thermal field was still not completely mixed, and there were some temperature fluctuations at the jet exit. We will show that because of this the thermal field initially developed faster than for the usual heated jet experiments, but soon (by $x/D_j = 15$) the results were similar to those of previous experiments.

For the dispersion experiments with the fine rings, the jet diameter, D_j, was 30 mm and the jet exit velocity, U_j, was 9 m s^{-1}. For the heated jet experiments, U_j was varied from 4.5 to 18 m s^{-1} for $D_j = 15$ mm and was kept constant at 7 m s^{-1} for some experiments with a 6 mm jet. The main flow parameters are given in table 1. The temperature of the heated jet at the exit, T_j, was 10 °C above the ambient. As the flow evolves buoyancy effects become important. We used the criterion given by Chen & Rodi (1980) to determine the non-buoyant region of the jet. They showed experimentally that in order for the flow to remain passive, the relation, $F^{-1/2}(\rho_j/\rho_a)^{-1/4}x/D_j < 0.5$, must hold. Here $F \equiv U_j^2\rho_j/gD_j(\rho_a - \rho_j)$ is the Froude number and g, ρ_j and ρ_a are the gravitational acceleration, air density at the jet exit and density of ambient air respectively. The non-buoyant regions for our heated jet experiment were $x/D_j < 127$ for $U_j = 18$ m s^{-1}, $x/D_j < 63$ for $U_j = 9$ m s^{-1} and $x/D_j < 32$ for $U_j = 4.5$ m s^{-1}. The measurements were made mainly at $x/D_j = 40$ for 18 and 9 m s^{-1} and at $x/D_j = 30$ for 4.5 m s^{-1}, well within the passive region.

The mean temperature was measured with a chromal–constantan thermocouple. The temperature fluctuations were measured with platinum resistant wires of diameter 1.25 μm for the experiments when the jet Reynolds number, $Re_j = U_j D_j/\nu$, was 9000

D_j (mm)	U_j (m s^{-1})	x/D_j	Re_j	$l_{1/2}$ (mm)	Re_l	R_λ	η (mm)	$l_{\theta_{1/2}}$ (mm)
30	9	9	18000	28	2300	190	0.08	—
15	18	40	18000	60	2600	198	0.17	70
15	9	40	9000	60	1230	136	0.29	70
15	. 4.5	30	4500	—	—	—	—	—
6	7	30	2800	—	—	—	—	—

TABLE 1. Velocity characteristics. Here U_j is the jet exit velocity, D_j is the jet diameter, x/D_j is the measurement position, $l_{1/2}$ is the jet half-width at the measurement location and $l_{\theta_{1/2}}$ is the mean temperature half-width for the heated jet experiments. $Re_j \equiv U_j D_j/\nu$ is the jet Reynolds number, where ν is the kinematic viscosity (1.5×10^{-5} m^2 s^{-1}). $Re_l \equiv \langle u^2 \rangle^{1/2} l_{1/2}/\nu$ is the turbulent Reynolds number, where $\langle u^2 \rangle^{1/2}$ is the longitudinal r.m.s. velocity. The microscale Reynolds number, $R_\lambda \equiv \langle u^2 \rangle^{1/2} \lambda/\nu$, where λ, the Taylor microscale, is determined from the longitudinal velocity derivative. The Kolmogorov scale, η, is $l_{1/2} Re_{l_{1/2}}^{-3/4}$. The blank spaces are unmeasured parameters.

or lower and 0.625 μm for the measurements at $Re_j = 18000$. The wire length to diameter ratio was approximately 500 in both cases. In order to measure temperature derivatives, a pair of carefully matched wires was used. The separation of the wires was 0.33 mm which corresponded to a ratio of $\Delta/\eta = 1.89$ at $x/D_j = 40$ for $Re_j = 18000$, where Δ and η are the wire separation and Kolmogorov scale respectively. The separation was chosen as a compromise between accurately determining the derivative and minimizing the correlation coefficient between the temperature fluctuations, θ, and the measured temperature difference, $\Delta\theta$, from which the derivative was determined. The derivative measurement requires the noise level to be low, and this increases relative to the signal when Δ is diminished (Antonia & Mi 1993). However, in order to correctly estimate the correlation between small- and large-scale quantities (i.e. temperature fluctuations and their dissipation), the cross-correlation between $\Delta\theta$ and θ, $\rho_{\Delta\theta,\theta}$, and thus Δ, should be as small as possible. Tong & Warhaft (1994*b*) show that $\rho_{\Delta\theta,\theta}$ increases linearly with Δ and is nearly 0.15 for $\Delta/\eta = 3$, a spacing often used by other workers. For the separation chosen here ($\Delta/\eta = 1.89$), $\rho_{\Delta\theta,\theta}$ was approximately 0.07 and the variance of the noise differences of the two wires was less than 10% of the signal differences, so no extrapolation was needed to infer statistics for small wire separations (as done by Antonia & Mi 1993). For all the Reynolds number studied ($Re_j =$ 2800–18000), the probe spacing was between 0.92η and 1.89η, thus the temperature field was well resolved. More details are given in Tong & Warhaft (1994*b*). Velocity fluctuations were measured with a TSI 1241 tungsten X-probe calibrated using a method due to Browne, Antonia & Chua (1989), in which a single effective angle between the streamwise direction and the wire was determined. The wires were operated with an overheat ratio 1.8 in conjunction with Dantec 55M01 anemometers. The separation between the X-wire and the temperature wire was about 1 mm. This is wider than the Kolmogorov scale but these measurements were only used to determine correlations at the integral scale (see §3.4). The velocity signal was offset before being amplified and the temperature signals were high-pass filtered. Then all signals were low-pass filtered to eliminate high-frequency noise and digitized with a 12 bit A/D converter. For most cases, 4×10^5 samples were taken for each data record. The sampling period was rapid for the spectra and coherence measurements (order of a Kolmogorov time period) but for the p.d.f. and conditional dissipation measurements it was slow (order of an integral scale). Here the samples must be independent of each other (Tennekes & Lumley 1972, Ch. 6).

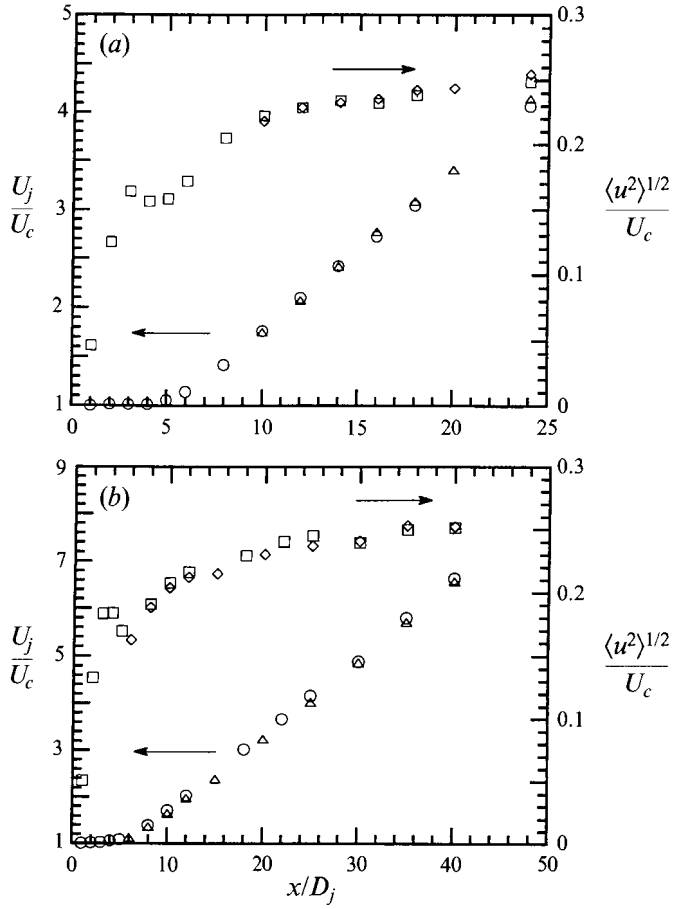

FIGURE 3. The normalized centreline velocity, U_j/U_c, and longitudinal turbulence intensity, $\langle u^2\rangle^{1/2}/U_c$, as a function of normalized downstream distance, x/D_j. (*a*) $D_j = 30$ mm, $U_j = 9$ m s^{-1}, $Re_j = 18000$. (*b*) $D_j = 15$ mm, $U_j = 18$ m s^{-1}, $Re_j = 18000$. For case (*a*) a 30 mm ring was placed in the flow at $x/D_j = 9$ and for case (*b*) a 15 mm ring was placed in the flow at $x/D_j = 4$. Profiles were also measured without the ring in the flow. ○, U_j/U_c no ring; △, U_j/U_c with ring; □, $\langle u^2\rangle^{1/2}/U_c$ no ring; ◇, $\langle u^2\rangle^{1/2}/U_c$ with ring.

3. Results

3.1. *Flow conditions*

Before outlining the results of the scalar dispersion and mixing, we will describe the characteristics of the velocity field.

The mean and r.m.s. longitudinal velocity along the jet centreline are shown in figure 3 for $D_j = 30$ mm, $U_j = 9$ m s^{-1} (figure 3*a*) and $D_j = 15$ mm, $U_j = 18$ m s^{-1} (figure 3*b*). Re_j is 18000 for both cases (table 1). In the self-similar region ($x/D_j \geqslant 8$), the centreline mean velocity decays as $U_c = 6.13U_j[(x-x_0)/D_j]^{-1}$ where U_c is the streamwise mean velocity on the jet centreline and x_0 is the virtual origin of the jet. The decay constant is close to the value of 6.2 given by Chen & Rodi (1980). Notice that while self-similarity for the mean velocity occurs by $x/D_j \approx 8$, it takes longer for the longitudinal turbulent intensity, $\langle u^2\rangle^{1/2}/U_c$, where $\langle u^2\rangle^{1/2}$ is the longitudinal r.m.s. velocity, to reach its asymptotic value of around 0.25. Figure 3(*a*) also shows that the rings used to introduce temperature fluctuations into the jet do not have significant effects on the

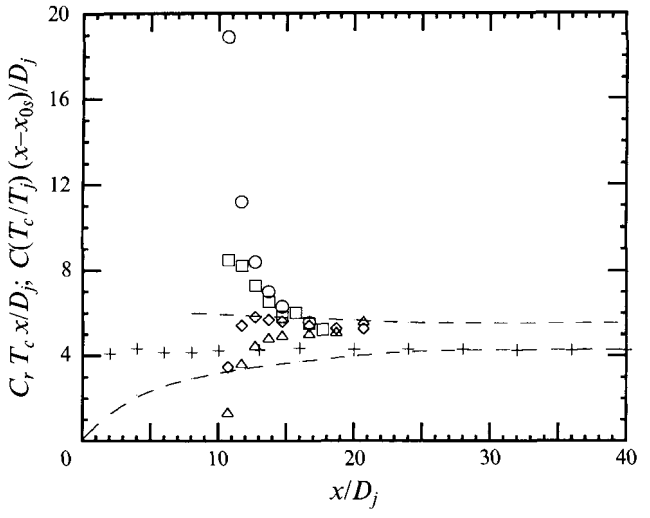

FIGURE 4. The evolution of the centreline mean temperature. For the rings, $C_r T_c x/D_j$ is plotted as a function of x/D_j, while for the heated jet the plot is of $C(T_c/T_j)(x-x_{0s})/D_j$. See the text for the definitions. The rings were placed at $x/D_j = 9$ in the 30 mm jet; $U_j = 9$ m s^{-1}. ○, 10 mm ring; □, 20 mm ring; ◇, 30 mm ring; △, 40 mm ring; +, our heated jet experiment ($U_j = 18$ m s^{-1}, $D_j = 15$ mm); ---, the spread of previous jet data compiled by Dowling & Dimotakis (1990).

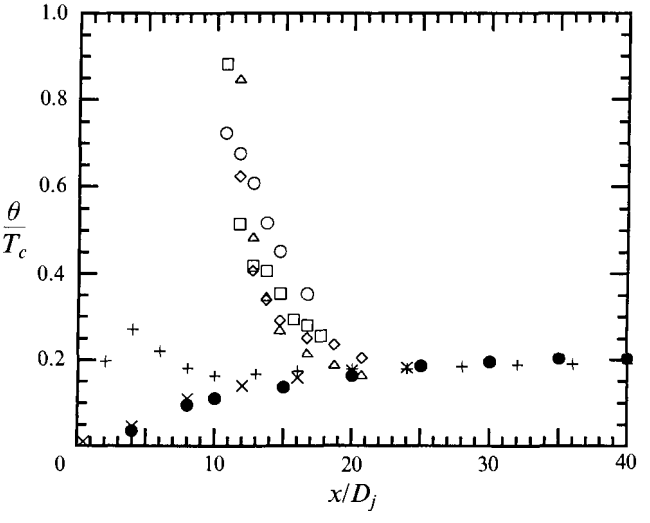

FIGURE 5. The evolution of the centreline scalar fluctuation intensity, θ/T_c. The open symbols are for the same conditions as figure 4. The crosses are the average values taken from previous jet data compiled by Dowling & Dimotakis (1990) and the filled circles are from the Lockwood & Moneib (1980) heated jet experiments. Our own heated jet experiments are the plus signs.

velocity field when placed at $x/D_j = 9$. The effect of the rings on the velocity field when placed closer to the jet is discussed in Tong & Warhaft (1994*a*). The velocity profile at the jet exit was close to top-hat and the fluctuation intensity was about 0.1%. Transverse profiles at different downstream locations in the self-similar region (not shown here) were in good agreement with those in literature (Wygnanski & Fiedler 1969; Panchapakesan & Lumley 1993; Hussein, Capp & George 1994).

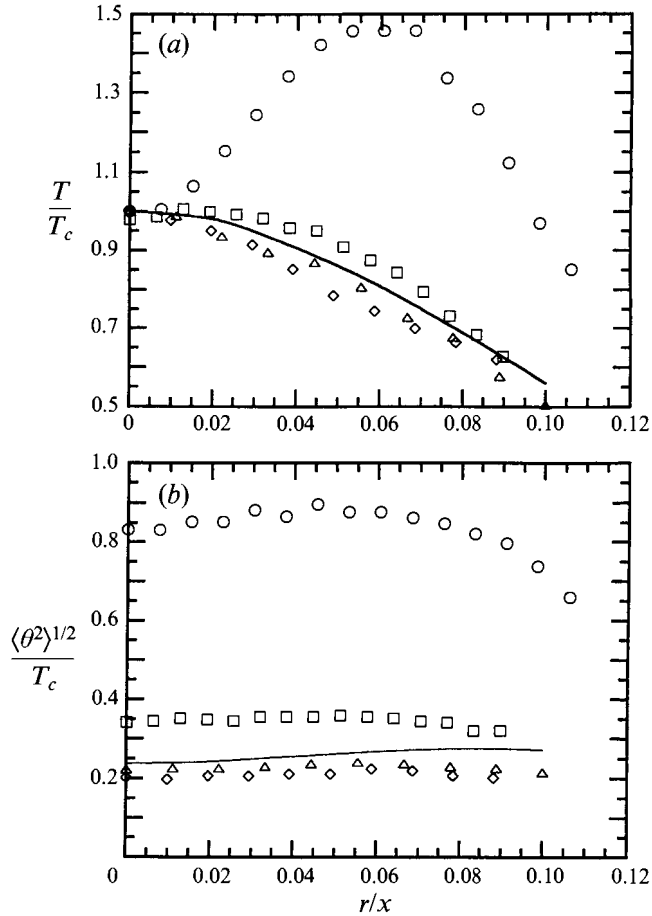

FIGURE 6. (*a*) Transverse mean temperature profiles and (*b*) transverse r.m.s. temperature profiles at various x/D_j for a 40 mm ring placed at $x/D_j = 9$. $D_j = 30$ mm and $U_j = 9$ m s^{-1}. ○, $x/D_j = 11$; □, $x/D_j = 13$; △, $x/D_j = 15$; ◇, $x/D_j = 17$. The line is the data from Dowling & Dimotakis (1990), measured in the self-similar region ($30 \leqslant x/D_j \leqslant 90$).

3.2. *Dispersion from a single source*

The evolution of the mean temperature, T_c, along the jet centreline (relative to the ambient surroundings) for rings of different diameters located at $x/D_j = 9$ for $D_j =$ 30 mm is shown in figure 4. Also plotted are the results of the 15 mm heated jet, and the upper and lower boundaries of results from different heated jet and concentration experiments compiled by Dowling & Dimotakis (1990). For these mean temperature (or concentration) measurements Dowling & Dimotakis plotted their results in the form $(T_c/T_j)(x-x_{0s})/D_j$, where x_{0s} is the virtual origin for the scalar field (which is close to that of the velocity). This scaling produces a horizontal line in the fully developed region. Since in the self-similar region the scalar spreads at the same rate as the jet, the value of the ordinate corresponds to the decay constant, C, of mean temperature, defined by $T_c = CT_j[(x-x_{0s})/D_j]^{-1}$.

The thermal field close to the rings was quite different from that of the heated jet, with very high initial mean values. Thus we adopted a slightly different scaling, plotting the ordinate as $C_r T_c x/D_j$, and selecting the constant C_r such that the mean temperature fell in the same range as the heated jet in the self-similar region. The selection of C_r

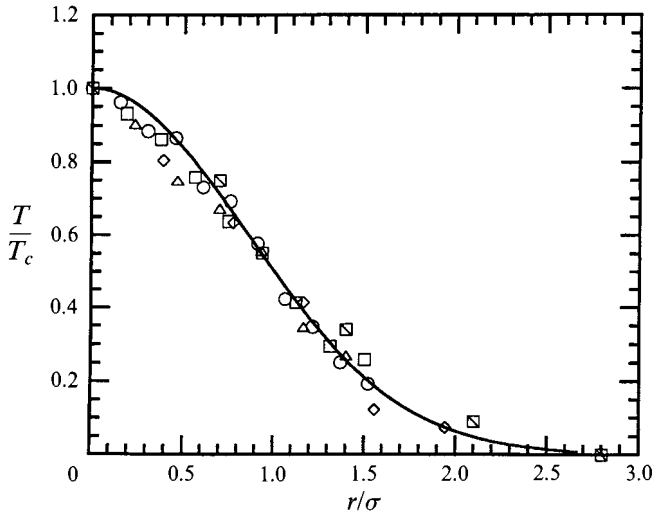

FIGURE 7. Transverse mean temperature profiles for the approximate point-source experiment. A 2 mm ring was placed at $x/D_j = 9$ ($U_j = 9$ m s^{-1}, $D_j = 30$ mm). The measurement locations are: □, $x/D_j = 10$; ◇, $x/D_j = 10.7$; △, $x/D_j = 11.7$; □, $x/D_j = 13$; ○, $x/D_j = 14$. The transverse distance has been normalized by the mean thermal field half-width, σ. A Gaussian curve is shown as a solid line.

effectively matches the heat flux of the various experiments. While the temperature is high immediately downstream of the small rings (10 and 20 mm diameter), it approaches a horizontal line at $x/D_j \approx 20$ (with the larger ring reaching it quicker) suggesting that at this location the mean field is similar to that of the heated jet experiment. The low initial value for the 30 and 40 mm rings are because, for these large-diameter rings, the peak mean temperatures occur off the jet centreline before they merge by $x/D_j \approx 13$ (see figure 6*a*, below).

The results for our heated jet experiment are also shown in figure 4. As mentioned in §2, the resistance ribbon in the plenum used to heat the air produced considerable fluctuations which had not vanished by the jet exit. Thus our results show greater initial value for both mean and r.m.s. temperature than does previous work. However, by $x/D_j \approx 15$ the mean field has become self-similar, well before the region of interest for the study of mixing in the far field (§3.4). We scaled the results in the same way as Dowling & Dimotakis (1990) and the mean temperature decay constant was found to be 4.3.

The temperature fluctuation intensity on the jet centreline, $\langle\theta^2\rangle^{1/2}/T_c$, for the cases just discussed, is plotted in figure 5, and again compared with the results from the average values of data compiled by Dowling & Dimotakis (1990), and with the experiment of Lockwood & Moneib (1980). Most workers with heated jets obtain an asymptotic value of 0.21 ± 0.03 in the self-similar region. Close to the rings, as would be expected, a very high fluctuation intensity is produced, but it decreases quickly and by $x/D_j \approx 20$ it approaches the value observed for heated jets. This is approximately the same location at which the mean temperature became self-similar (figure 4). The results for smaller rings show a similar trend to the larger ones although it takes longer for them to reach the asymptotic value. Our heated jet results have a higher temperature fluctuation intensity in the developing region due to the reason mentioned in the previous paragraph. However, its asymptotic value of approximately 0.2, is close to other heated jet experiments. (The fact that it appears to reach the self-similar values

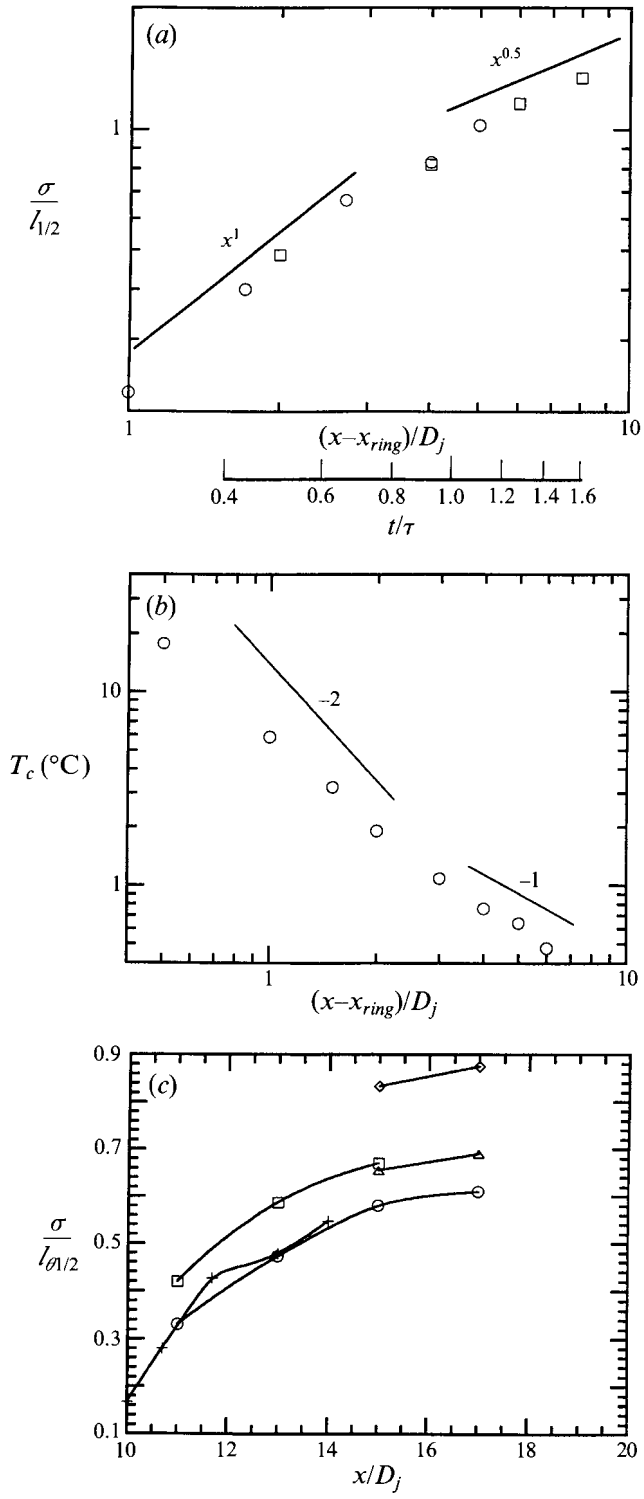

FIGURE 8. (*a*) The downstream evolution of the half-width of the mean temperature profiles for the point source (circles, same flow conditions as figure 7) and a 10 mm ring (squares) also placed at $x/D_j = 9$ ($U_j = 9$ m s^{-1}, $D_j = 30$ mm). The half-width has been normalized by the half-width of the jet determined at $x/D_j = 9$. The position of the ring is x_{ring} and t/τ is the time measured in eddy

for mean and r.m.s. temperature at approximately $x/D_j = 10$, somewhat earlier than the previous heated jet experiments, appears to be associated with the incomplete mixing in the plenum.)

The transverse profiles of mean and r.m.s. temperature, T and $\langle\theta^2\rangle^{1/2}$, for the 40 mm ring, normalized by the centreline mean are plotted in figures 6(*a*) and 6(*b*). For this diameter ring, the ratio of the radius of the ring to the half-width of the jet at the ring location, $r_{ring}/l_{1/2}$, is 0.71. Initially, at $x/D_j = 11$, the mean profile has a peak above the ring. The peaks on the circumference then expand and merge and the profile becomes close to that of the heated jet. The r.m.s. temperature profiles (figure 6*b*) are relatively flat and the shape does not change significantly for $x/D_j > 13$. In the self-similar region their value is slightly lower than the data of Dowling & Dimotakis (1990).

In figure 7 we show the mean profiles for the very small ring (2 mm diameter) which was intended to approximate a point source. The ring was placed at $x/D_j = 9$, on the jet centreline. The radial distance has been normalized by the half-width of each profile. For all the downstream locations the profiles appear to be self-similar and close to Gaussian, although there is some scatter. Gaussian profiles have also been found for a line source of the centreline of a plane jet (Paranthoen *et al.* 1988). They are observed because close to the jet centreline the flow is approximately homogeneous and the mean shear is small. The half-width of these mean profiles, σ, normalized by the jet half-width at $x/D_j = 9$, are plotted against the distance from the source in figure 8(*a*). Also plotted the half-width for the 10 mm ring placed at $x/D_j = 9$. It is essentially the same as for the point source for $(x-x_{ring})/D_j > 2$. The initial linear growth (from $(x-x_{ring})/D_j = 1$ to 3) is similar to that for the turbulent–convective range of dispersion in isotropic turbulence. In this range, $\kappa/\langle v^2\rangle \ll t \ll t_L$ (Taylor 1921; Anand & Pope 1985; Warhaft 1984; Stapountzis *et al.* 1986), where t_L, t and v are the Lagrangian timescale, the diffusion time and the fluctuation velocity component in the cross-stream direction respectively. Here the diffusion time is small so the Lagrangian velocities are almost perfectly correlated, thus $\sigma \sim t$. Beyond $(x-x_{ring})/D_j = 5$, the half-width increases as $(x-x_{ring})^{0.5} \sim t^{0.5}$. This is the same spreading rate as the turbulent–diffusive range ($t \gg t_L$) in stationary isotropic turbulence (Taylor 1921; Warhaft 1984; Anand & Pope 1985; Stapountzis *et al.* 1986). It needs to be emphasized that in evolving flows such as free shear flows and decaying grid turbulence, turbulence disperses the scalar as well as its own lengthscale (Tennekes & Lumley 1972). Therefore, once the integral lengthscale of the scalar grows to the same order of the velocity field, it keeps pace with the velocity. Thus the observed growth of the half-width for $(x-x_{ring})/D_j > 5$, in a way consistent with the turbulent diffusion range, is really due to the growth of the integral scale of the velocity field which also spreads at $t^{0.5}$ since $U_c \sim x^{-1}$. Note that the diffusion time, t, from the position of the ring to $(x-x_{ring})/D_j = 5$ (where the slope changes from 1 to 0.5), is approximately one eddy turnover time, τ, defined as $l/\langle u^2\rangle^{1/2}$ where l is the integral lengthscale. (The diffusion time measured in eddy turnover time units (t/τ) is determined as $\int_{x_{ring}}^{x} (\langle u^2\rangle^{1/2}/l)\,\mathrm{d}x/U_c(x)$, where l is taken to be $l_{1/2}$.) Thus the dispersion is rapid. The evolution of the peak mean temperature for the point source is plotted in figure 8(*b*), which shows a two-stage power law decay. This is to be expected because the plume half-width has two stages of growth and the heat flux must be conserved. The decay

turnover time units. (*b*) The evolution of the centreline mean temperature for the point source. Same flow conditions as (*a*). (*c*) The half-width of the mean profiles for various rings placed at $x/D_j = 9$ ($U_j = 9$ m s^{-1}, $D_j = 30$ mm). The half-width at each downstream position has been normalized by that of the heated jet at the same location. The ring diameters are: ○, 10 mm; □, 20 mm; △, 30 mm; ◇, 40 mm. These are compared with the same point source (+) as in (*a*).

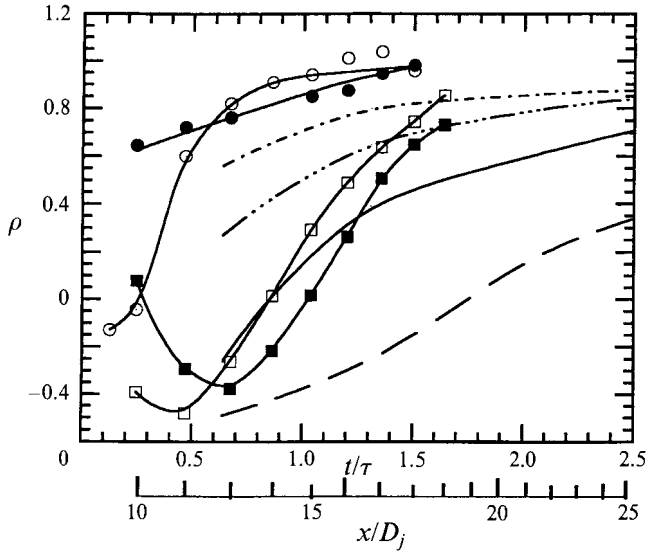

FIGURE 9. The evolution of the cross-correlation coefficient, ρ, as a function of x/D_j and t/τ, for the jet with two rings compared with two line sources in grid turbulence. For the rings in the jet, $D_j = 30$ mm, $U_j = 9$ m s^{-1} and the ring pairs were placed at $x/D_j = 9$. Their diameters were: ●, 35, 40 mm; ■, 20, 40 mm; ○, 10, 15 mm; □, 10, 30 mm. For the grid turbulence the mean velocity was 7 m s^{-1}, and the wires were placed at $x/M = 20$, where M (2.54 cm) is the grid mesh size, and the wire spacing is in terms of the integral scale of the turbulence, l. For these measurements the plot is as a function of t/τ only. The normalized wire spacing, d/l, was: —·—, 0.12; —·····—, 0.24; ——, 0.39; — — —, 0.78.

exponent for the turbulent–convective range is approximately 1.5. (In a flow with a constant mean velocity such as grid turbulence, this decay exponent would be -2, indicated by a solid line in the figure.) Farther downstream, the decay exponent becomes -1, the same as that of a heated jet (with different origin). Paranthoen *et al.* 1988) also observed a two-stage power law decay for a line source in a plane jet. The half-width for rings of different sizes, normalized by those of the heated jet, are shown in figure 8(*c*). For larger rings the half-width is greater than for the smaller ones since the large ring is located in the shear layer so the thermal wakes are dispersed faster. This is consistent with the observation that the mean and r.m.s. temperature also approaches that of the heated jet more quickly (figures 4 and 5). Note that for the 40 mm ring the half-width is very close to 1 (i.e. to that that of the heated jet) by $x/D_j = 17$. Although the power input to the smaller rings did not allow us to measure further downstream, we expect that these half-widths would also approach that of the heated jet.

3.3. *Mixing in the near field*

We now turn to the mixing of two scalars introduced independently into the jet. As discussed in the introduction, we divided the mixing into two stages, which are defined in terms of the correlation coefficient, ρ, between the two scalars. We begin with the near field ($\rho < 1$) and use the inference method of Warhaft (1981, 1984) to determine ρ. Here two heated rings are placed in the jet as sources of temperature fluctuations (figure 1). In order to determine the mixing, the measurement procedure needs to resolve the smallest scale in the flow for both scalars simultaneously. This is normally difficult to achieve since it requires two sensors (one for each scalar) that can measure to the Kolmogorov–Corrsin (or Batchelor) scale, and their separation must also not be

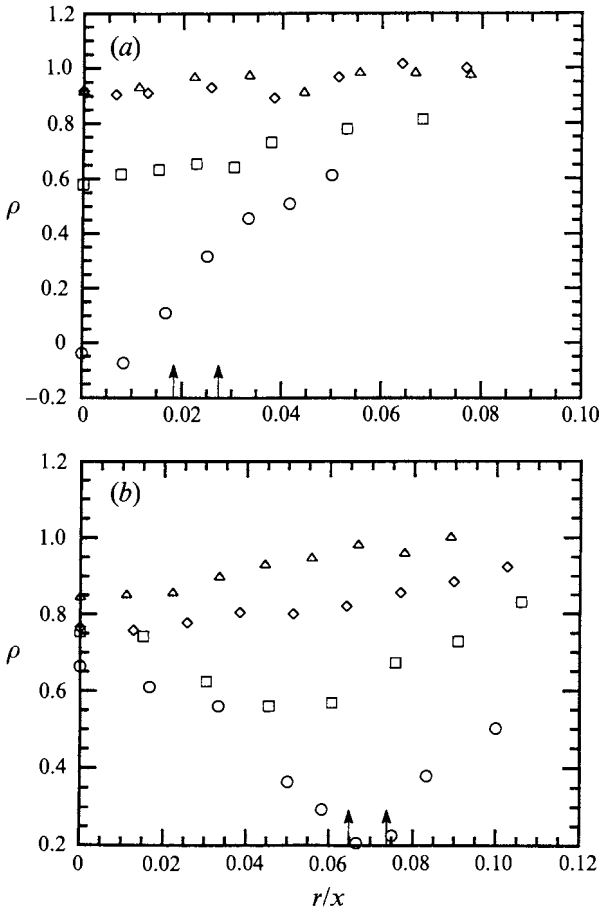

FIGURE 10. Transverse profiles of ρ for the 10, 15 mm ring pair (*a*) and the 35, 40 mm ring pair (*b*). $D_j = 30$ mm, $U_j = 9$ m s^{-1} and the ring pairs were placed at $x/D_j = 9$. The various downstream distances where the profiles were measured are: ○, $x/D_j = 10$; □, $x/D_j = 11$; ◇, $x/D_j = 13$; △, $x/D_j = 15$. The arrows show the radial positions of the rings.

bigger than these scales. The inference method, on the other hand, only requires the fine-scale measurement of one scalar (in this case temperature). It relies on the superposition of passive scalars (due to the linearity of the scalar diffusion equation) to determine the second-order statistics such as the covariance, $\langle \theta_A \theta_B \rangle$, and the co-spectrum. The method is outlined in the introduction, and in Warhaft (1981, 1984). Note that while the cross-correlation and coherence can be determined by this method, phase information is lost (since the measurements are not simultaneous) and thus the phase spectrum cannot be determined. Figure 9 shows the correlation coefficient of temperature fluctuation θ_A and θ_B, $\rho \equiv \langle \theta_A, \theta_B \rangle / (\langle \theta_A^2 \rangle \langle \theta_B^2 \rangle)^{1/2}$, along the jet centreline, for different combinations of ring diameters. The results from line sources in grid turbulence from Warhaft (1984) are also plotted for comparison. The distance from the sources is measured in eddy turnover time units, t/τ, as well as in terms of x/D_j. The correlation approaches unity, where the scalars are well mixed, for all cases. For the 10, 15 mm and 35, 40 mm ring pairs, the difference between the ring diameters, Δr, is small ($\Delta r/l_{1/2} = 0.167$). Here ρ attains high values very fast, especially for the 35, 40 mm pair, where ρ is 0.65 by $t = 0.25\tau$. But for the large spacing, $\Delta r/l_{1/2} = 0.51$ (10,

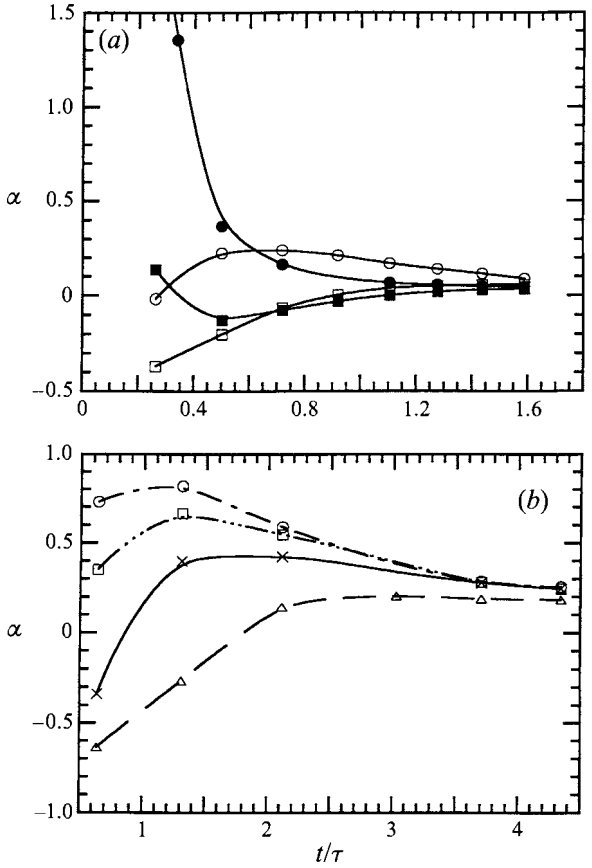

FIGURE 11. The segregation parameter, α, for various ring combinations in the jet (*a*) and in grid-generated turbulence, (*b*). The initial conditions and the symbols for the ring diameters are the same as for figure 9.

30 mm and 20, 40 mm ring pairs) ρ starts from close to zero and becomes negative before increasing towards unity. Here the thermal wakes are initially flapped in unison (producing negative correlation) before mixing produces the positive correlation. For all cases, the scalars are well mixed in the order of one eddy turnover time, which is also the period of rapid dispersion of a single scalar, as shown in §3.2. The qualitative evolution of ρ is similar to the observations of Warhaft (1984) in grid turbulence, also shown in figure 9. However, for the jet ρ evolves faster than in grid turbulence for comparable source separations. This is apparently due to the action of mean shear. Kerstein (1992) using his linear eddy model finds trends in ρ very similar to those shown in figure 9, but the evolution time is much longer.

Typical transverse profiles of ρ are shown in figures 10(*a*) and 10(*b*) respectively for the 10, 15 mm ring pair and the 35, 40 mm ring pair. In figure 10(*a*), close to the rings, ρ increases towards the edge of the jet, suggesting better mixing due to the shear. Farther downstream the profiles become flat and the correlation is close to unity across the jet. For large ring diameters, measurements at $x/D_j = 10$ show a minimum ρ at $r/x = 0.07$ (figure 10*b*), which is approximately the radial position of the ring wires (indicated by the arrows in the figure). This shows that there is weak mixing close to the sources. Apparently, the high initial correlation observed on the centreline for this case (figure 10*b*) is because it is physically farther from the sources, and thus the scalars

have time to partially mix before they reach the centreline. Note that the minimum values of ρ on the transverse profiles at $x/D_j = 10$ for small (10, 15 mm, figure 10*a*) and large ring pairs (35, 40 mm, figure 10*b*) are -0.1 and 0.2 respectively, indicating that the scalars are better mixed close to the sources for large rings at the same downstream location, owing to the presence of mean shear. Komori *et al.* (1991) also found that the shear increased mixing in their simulations based on a random flight model.

As discussed in the Introduction, another important parameter in turbulent mixing is the segregation parameter, α, defined as $\langle\theta_A\,\theta_B\rangle/T_A\,T_B$. Figure 11(*a*) shows α along the jet centreline for the four different ring combinations for which ρ was measured (figures 9 and 10). Data calculated from Warhaft (1984) are given in figure 11(*b*) for comparison. For the jet experiments, we expect that α will approach an asymptotic value of approximately 0.04, since $\langle\theta^2\rangle^{1/2}/T_c \to 0.2$ (figure 5) and $\rho \to 1$. The asymptotic trend of our measurements (figure 11*a*) is consistent with this value. In a similar way to ρ, α also has higher values for small $\Delta r/l_{1/2}$ (figure 11*a*). But the evolution of α, especially close to the rings, is different for small (10, 15 mm) and large (35, 40 mm) ring diameters. For the 35, 40 mm ring pair, α is initially very high, owing to the large temperature fluctuation intensity close to the rings. It then drops and approaches its asymptotic value. For the 10, 15 mm ring pair, α increases initially and then decreases. The curves for α in grid turbulence (figure 11*b*) have similar shapes to the small ring (10, 15 mm and 10, 30 mm) cases in the jet, but the development is slower. They take 3τ to 3.5τ to reach their asymptotic value of 0.2 compared to about 1.5τ for the jet. In figures 12(*a*) and 12(*b*) the transverse profiles of α are plotted at several downstream locations. Close to the rings, in a similar way to the correlation coefficient (figure 10), α is higher towards the edge, but the profile does not become flat far downstream since, although ρ is unity across the whole jet, the temperature fluctuation intensity is higher in the shear layer than at the centre.

Komori *et al.* (1991), using a random flight model, find that $\alpha \to 0$ with time in non-premixed homogeneous turbulence (α is -1 initially). This result is not inconsistent with our asymptotic value of 0.04, although we emphasize that the asymptotic value of α is dependent on the type of flow (unlike ρ). There have been other determinations of α in grid turbulence (Bennani, Gence & Mathieu 1985), in counterflowing jets (Mudford & Bilger 1984), and in a two-dimensional plume in the atmospheric surface layer (Komori, Ueda & Tsukushi 1985). In these studies the asymptotic values of α varied from slightly negative values, to -0.7. The simulations of Komori *et al.* (1991) as well as the theoretical considerations of Bilger, Mudford & Atkinson (1985) indicate that α can be positive, as our experiments also show.

The correlation coefficient and segregation parameter provide a bulk measure of mixing, but contain no scale information. However, mixing is a decidedly multi-scale process, with turbulence acting at the large and intermediate scales, and molecular diffusion smearing and completing the mixing at the smallest scales. Thus the correlation can become positive only when the scalars are mixed at molecular level, because otherwise $\langle(T_A+\theta_A)(T_B+\theta_B)\rangle = 0$, and thus $\langle\theta_A\,\theta_B\rangle$ is negative. Therefore, studying the mixing at different scales is necessary for a complete understanding of the mixing process. The scale information of the correlation as a function of wavenumber (or frequency, which is used here) can be obtained from the coherence of the two scalars. This was calculated by inferring the co-spectrum from the power spectra for each ring ($\Phi_{\theta_A}(f)$ and $\Phi_{\theta_B}(f)$) and both rings operating together, $\Phi_{\theta_{A+B}}(f)$, i.e. $Co_{\theta_A\theta_B}(f) = [\Phi_{\theta_{A+B}}(f) - \Phi_{\theta_A}(f) - \Phi_{\theta_B}(f)]/2$.

The coherency spectra, $\rho(f) = Co_{\theta_A\theta_B}(f)/[\Phi_{\theta_A}(f)\,\Phi_{\theta_B}(f)]^{1/2}$, and co-spectra for the 10, 20 mm ring pair measured at different downstream locations along the jet centreline

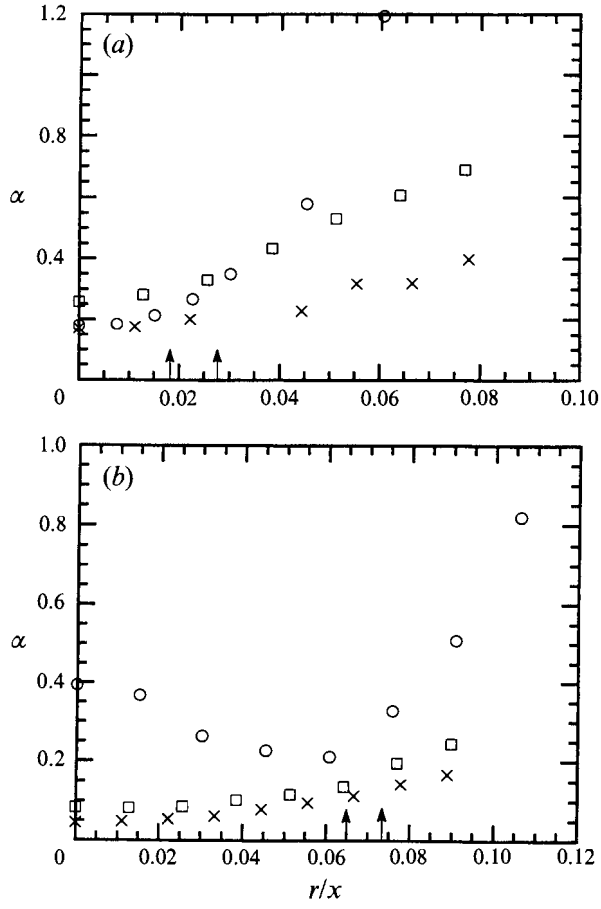

FIGURE 12. The transverse profiles of α for two sets of ring pairs: (*a*) 10, 15 mm diameter rings and (*b*) 35, 40 mm diameter rings. $D_j = 30$ mm, $U_j = 9$ m s^{-1} and the rings were at $x/D_j = 9$. The measurement locations were: ○, $x/D_j = 11$; □, $x/D_j = 13$; ×, $x/D_j = 15$. The arrows show the radial positions of the rings.

are plotted in figures 13(*a*) and 13(*b*) respectively. Close to the sources ($x/D_j = 9.5$) the two thermal wakes are unmixed and the probe sees unheated air most of the time, and $\rho(f)$ is close to zero at all scales. As they are convected downstream the scalars are flapped and stirred by the large-scale motion and the probe spends a considerable fraction of time in one scalar field or the other, but not generally in both fields together, since they are poorly mixed. This produces a negative coherence (of value of approximately -0.55 at $x/D_j = 10$) at low frequencies. Since the structure of the temperature field is coarse at this point, $\rho(f)$ is still close to zero at the small scales. As the scalar fields evolve, their structure becomes finer, i.e. the coherence is transferred to the small scales. Thus the small scales, like the large ones, become negatively correlated. Here, too, the probe is mainly sampling one scalar or the other but rarely both together ($x/D_j = 10.3$). Farther downstream, while $\rho(f)$ is still decreasing at the small scales, the entrainment of the ambient air by the jet starts to produce similar structures in both scalar fields, and thus $\rho(f)$ tends towards positive values at large scales (x/D_j varying from 10.3 to 11, figure 13(*a*)). The positive coherence is then transferred to the small scales and finally $\rho(f)$, approaches unity at all scales ($x/D_j =$

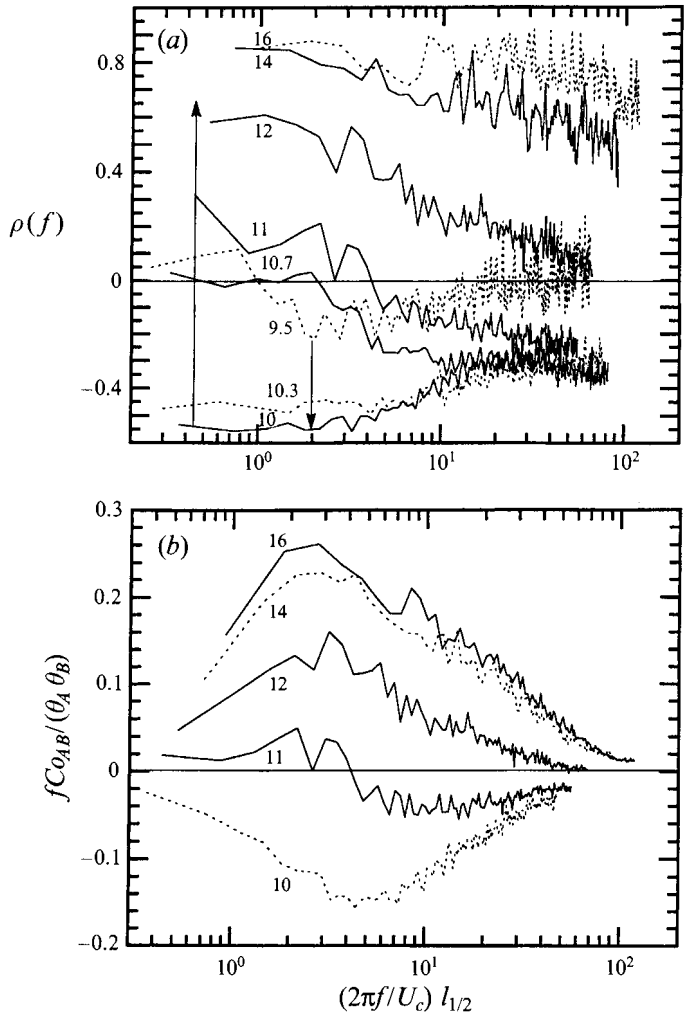

FIGURE 13. The coherence (*a*), and amplitude co-spectrum (*b*), for the 10, 20 mm ring pair placed at $x/D_j = 9$. $D_j = 30$ mm, $U_j = 9$ m s^{-1}. The measurements at various x/D_j were along the jet centreline. The measurement positions (x/D_j) are given on the graphs. $l_{1/2}$ is the jet half-width and f is frequency (Hz).

16). We see that in the evolution of $\rho(f)$, the small scales lag behind the large scales. This is especially evident for x/D_j between 10.7 and 14. The co-spectra are shown in figure 13(*b*). The integral of the co-spectrum is the cross-correlation coefficient, ρ. For $x/D_j < 10$ and > 12, the co-spectrum has the same sign at all frequencies. Here the contribution to ρ is mostly from large scales. Thus in these ranges ρ (figure 9) evolves in a similar way to $\rho(f)$ and the co-spectrum at large scales (low frequencies). However, for the intermediate range ($x/D_j \sim 11$) the co-spectrum changes sign and the value of ρ is influenced by both large and small scales. The evolution of the coherence for different ring sizes, and along a ray at an angle with the centreline (not shown here), follows the same qualitative course as figure 13.

While our main focus is on mixing of scalars introduced into the jet in the self-similar region, and at the same downstream location, we also present in figure 14 some results for cases with different initial conditions. These are: (*a*) the mixing of temperature

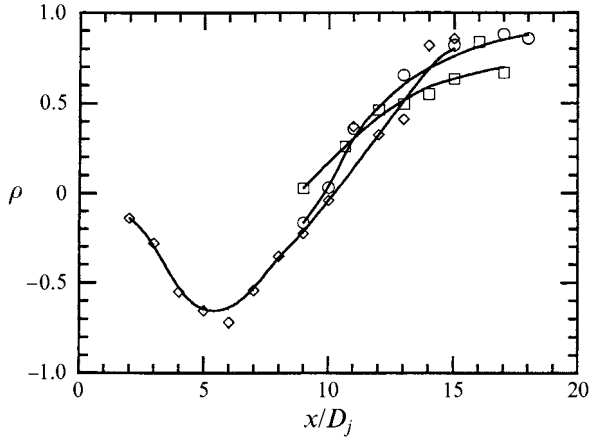

FIGURE 14. The downstream evolution of ρ for various other initial conditions: $\diamond$, 10, 20 mm rings placed close to the jet at $x/D_j = 0.5$; $\square$, a 20 mm diameter ring at $x/D_j = 2$ and a 30 mm diameter ring at $x/D_j = 7$; $\bigcirc$, a 30 mm diameter ring at $x/D_j = 7$ mixing with the heated jet. $D_j = 30$ mm, $U_j = 9$ m s^{-1}.

fluctuations from two rings placed close to the jet exit; (*b*) two rings separated longitudinally; and (*c*) fluctuations produced by one ring and the heated jet. The evolution of ρ for the 10, 20 mm ring pair close to the jet exit ($x/D_j = 0.5$) is similar to the cases shown in figure 9 for the rings in the self-similar region: initially the thin thermal fields from the two sources are flapped, causing the negative cross-correlation, and by $x/D_j = 5$ the mixing process begins, driving ρ to positive values. For the case of two rings with large separation in the streamwise direction (the first ring at $x/D_j = 2$ and the second at 7), the distance between the rings is larger than the integral lengthscale. Immediately downstream of the second ring the correlation of the two scalars is close to zero (figure 14). This is to be expected because, at the location of the second ring, the two thermal fields are in different stages of evolution, and thus their characteristic scales are quite different. The thermal field of the first ring is comparatively well developed and its fluctuations are mainly due to the entrainment of ambient air and turbulent stirring by the time it reaches the second ring. The thin thermal wake from the second ring, flapped by the large-scale motion, then encounters this well-mixed plume. Thus the thin thermal wake is quite independent of the well-mixed plume from the first ring, which is of scale l, and a zero cross-correlation thereby results. Farther downstream ρ increases monotonically, in a similar way to the cases we discussed before. Finally, in figure 14 we show the variation of ρ for the case of one ring placed at $x/D_j = 7$ in the heated jet. This situation is nearly identical to the case of the separated rings just discussed since, at the location of the ring, the heated jet is also relatively well mixed. Note the remarkable similarity of the evolution of ρ for the very different initial conditions of figure 14.

Finally, we note that mixing does not necessarily result in a positive correlation. In the case of two plumes in a jet or two line sources in grid turbulence, the uncontaminated (or unheated) ambient air is essential for both ρ and α to become positive. It can easily be shown that for a non-premixed ($\rho = -1$) non-reacting flow containing two adjacent scalar fields, ρ remains -1 for all time. Komori *et al.* (1991) have shown that $-1 \leqslant \alpha \leqslant 0$ for this case. In the case of dilute homogeneous scalar fields with equal Prandtl (or Schmidt) numbers, the evolution of the correlation coefficient depends on the correlation at large and small scales (Yeung & Pope 1993).

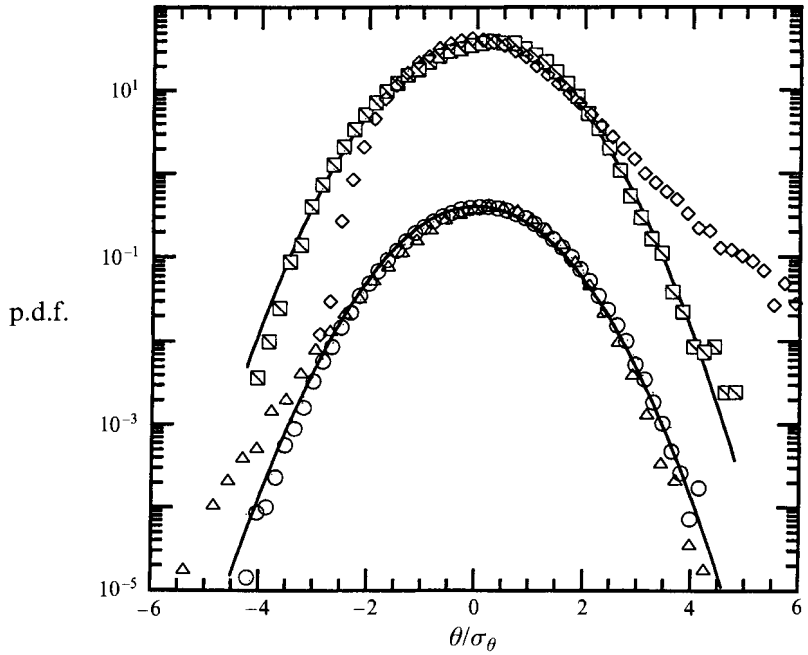

FIGURE 15. The p.d.f.'s of temperature fluctuations. The upper curves (shifted by two decades from the lower) are for a 10 mm ring placed at $x/D_j = 0.5$ ($D_j = 30$ mm. $U_j = 9$ m s^{-1}). The measurement locations are: ◇, $x/D_j = 10$; ⧅, $x/D_j = 15$. The lower curves are for the heated jet: △ and ○, measurements at $x/D_j = 24$ and $x/D_j = 40$ respectively ($D_j = 15$ mm, $U_j = 18$ m s^{-1}). The solid lines are Gaussian curves and all measurements are along the jet centreline.

For flows with fast (large Damköhler numbers) irreversible chemical reaction, the two scalars cannot coexist, therefore both α and ρ will remain negative.

3.4 *Mixing in the far field*

We have shown that as the temperature field introduced by the rings evolves, by about 1.5 eddy turnover times the mean and r.m.s. profiles become close to those of a self-similar heated jet. Here the thermal field has become independent of its initial conditions. By this position, if two scalars are introduced upstream (by means of two rings), they have become fully mixed with each other ($\rho = 1$). We define the far field of mixing as that region when ρ is unity. Here the mixing is between the heated jet and the cooler, ambient air.

Figure 15 shows the p.d.f.'s of temperature fluctuations on the jet centreline for the 10 mm ring placed at $x/D_j = 0.5$ in the 30 mm jet (i.e. very close to the jet exit), and for the 15 mm heated jet. Initially the p.d.f.'s are skewed in different ways. The ring has the expected extended tail (measured at $x/D_j = 10$) on the hot side (because of the hot spike at the ring), while the heated jet has its longer tail (measured at $x/D_j = 24$) on the cold side (due to the entrainment). However, farther downstream the p.d.f.'s are almost identical, and close to Gaussian (measured at $x/D_j = 15$ for the ring and $x/D_j = 40$ for the heated jet). Other initial conditions produced similar results. Figure 16 shows temperature p.d.f.'s off the jet centreline, in the far field. Both the heated jet and the ring produce p.d.f.'s that are skewed to the high-temperature side, showing that gusts of warm air from the jet are more probable than cool gusts of the same magnitude from the surroundings. These findings are consistent with the measurements of Venkataramani, Tutu & Chevray (1975) and Lockwood & Moneib (1980). We note

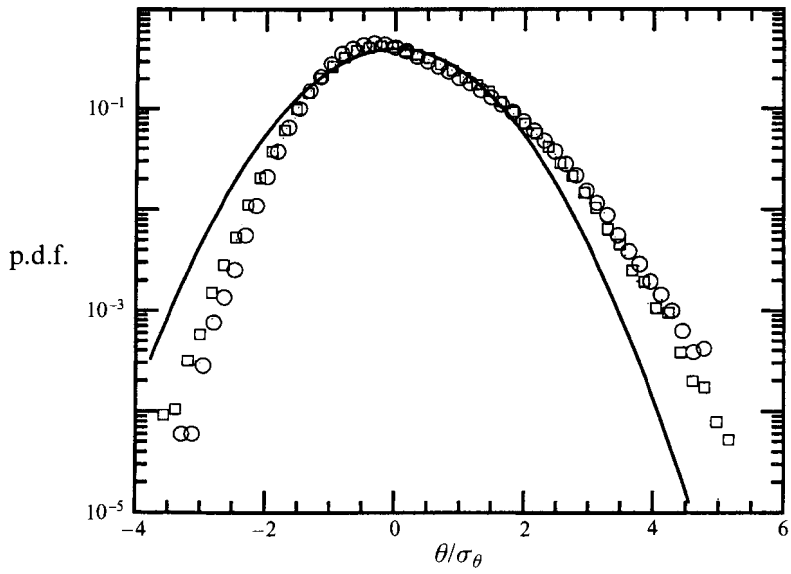

FIGURE 16. P.d.f.'s of the heated ring and the heated jet, off the centreline at $r/x = 0.11$. ○, heated jet measured at $x/D_j = 40$; □, heated ring (15 mm diameter placed at $x/D_j = 4$) measured at $x/D_j = 40$. $D_j = 15$ mm, $U_j = 18$ m s^{-1}. The solid curve is Gaussian.

that Sreenivasan, Antonia & Britz (1979) showed, in their heated jet experiment with co-flow, that off the jet centreline the p.d.f. of θ corresponded to 'superposed' turbulence, i.e. the temperature signal obtained by subtracting the ramp–cliff structures (to be discussed later in this section and in § 4) from the total signal was close to Gaussian. The typical instantaneous cross-stream scalar profiles, observed by Dahm & Dimotakis (1987) in water jets and by Uberoi & Singh (1975), Schefer *et al.* (1994) and Kerstein & Schefer (1994) in gaseous jets, show that the instantaneous concentrations of mixed fluid across the jet are often fairly uniform but with sharp edges, in contrast to what the mean profile might suggest. This is probably directly related to the ramp–cliff structure, providing a different perspective of the same object. This suggests that in regions separated by 'cliffs' the scalar is well mixed and the non-Gaussian p.d.f. is caused by these large-scale structures.

The spectra of the longitudinal velocity and temperature fluctuations in the far field are shown in figure 17. Here we have multiplied the ordinate of the raw spectra by f^n where f is the frequency and n is the scaling exponent. This method of plotting clearly displays the scaling region. The velocity and temperature spectra have scaling exponents of -1.47 and -1.37 respectively, extending a little more than a decade in frequency space. The temperature spectrum exponent at this $R_\lambda(\sim 200)$ is consistent with the results compiled by Sreenivasan (1991). We have not been able to find other measurements of the velocity spectrum at $R_\lambda \sim 200$. The jet results of Gibson (1962) at $R_\lambda = 750$, and Champagne (1978) at $R_\lambda = 600$, show a $-5/3$ scaling region. Our lower scaling exponent apparently reflects the lower R_λ of the measurements.

The statistics of temperature fluctuations, θ, and their difference, $\Delta\theta$, for the far field are given in table 2, and some of these are plotted in figures 18 and 19, to be discussed in a moment. The values of the skewness and kurtosis of θ (normalized third and fourth moments) are consistent with the previous results of Venkataramani *et al.* (1975) and Lockwood & Moneib (1980). They show no trend with Reynolds number. The temperature difference was measured in two directions: in the radial direction and 70°

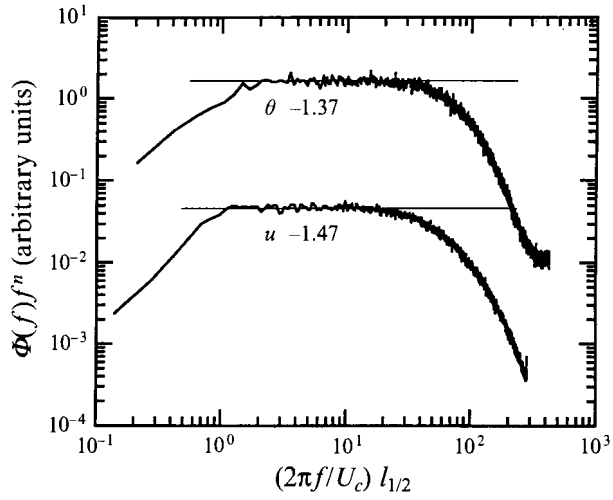

FIGURE 17. Temperature (upper curve) and velocity spectra measured in the far field of the scalar evolution. $D_j = 15$ mm, $U_j = 18$ m s^{-1} and the measurements were at $x/D_j = 40$ for the heated jet. The numbers show the scaling exponents.

U_j (m s^{-1})	Re_j	x/D_j	r/x	θ		Probe angle	$\Delta\theta$		ρ_p	$\rho_{\theta^2,(\Delta\theta)^2}$	$\rho_{\theta,(\Delta\theta)^2}$
				S	K		S	K			
18	18000	40	0	−0.16	2.98	0	0	14.5	0	0.02	−0.01
						70	−0.85	13	0.16	0.039	−0.075
9	9000	40	0	−0.18	3.04	0	0	13	0.0	0.002	−0.016
						70	−0.65	11	0.2	0.053	−0.064
4.5	4500	30	0	−0.04	3.0	0	0	7	0.06	0.02	−0.05
						70	−0.78	9.5	0.29	0.07	−0.06
18	18000	40	0.1	0.35	2.9	0	−1.3	15	0.2	0.04	0.07
						70	−1.24	14	0.25	0.06	0.06
9	9000	40	0.1	0.38	2.95	0	−1.2	12	0.12	0.04	0.02
						70	−0.98	10	0.03	0.015	−0.045
18	18000	40	0.15	0.82	4.5	0	−0.95	11	0.28	0.05	0.06
						70	−1.1	12	0.29	0.06	0.09
9	9000	40	0.15	0.7	4.2	0	−0.9	8.6	0.45	0.09	0.08
						70	−0.9	9.5	0.59	0.12	0.14
4.5	4500	30	0.15	0.74	4.3	0	−0.61	6	0.51	0.12	0.09
						70	−0.85	8	0.83	0.16	0.16
18	18000	40	0.17	0.9	5.0	0	−0.9	11	0.5	0.06	0.05
						70	−0.97	11.5	0.57	0.1	0.12
7	2800	30	0	—	—	0	—	—	0.14	0.03	−0.07
($D_j = 6$ mm)						70			0.11	0.02	−0.08
7	2800	30	0.15	—	—	0	—	—	0.64	0.1	0.1
($D_j = 6$ mm)						70			0.9	0.16	0.15

TABLE 2. Temperature statistics. Here θ is the temperature fluctuation, $\Delta\theta$ is the temperature difference, S and K are the skewness and kurtosis respectively, $\rho_{\theta^2,(\Delta\theta)^2}$ is the correlation coefficient between θ^2 and $(\Delta\theta)^2$, and $\rho_{\theta,(\Delta\theta)^2}$ is the correlation coefficient between θ and $(\Delta\theta)^2$, ρ_p is a correlation function defined as $\langle\theta^2(\Delta\theta)^2\rangle/(\langle\theta^2\rangle\langle(\Delta\theta)^2\rangle) - 1$ (see text). The radial position of the probe is r/x and the probe angle is measured from the radial plane (see figure 20 for sketches).

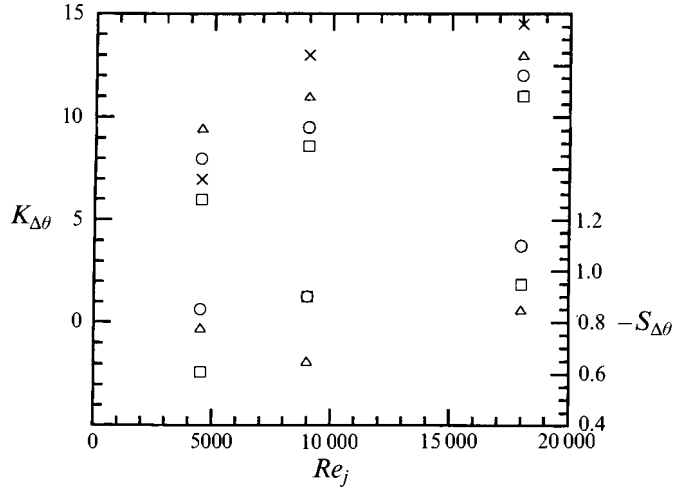

FIGURE 18. Higher-order statistics for the temperature difference, $\Delta\theta$, as a function of the jet Reynolds number. Upper points, the kurtosis; lower points, the skewness: ×, centreline measurements with the probe spacing in the radial plane; △, centreline with probe oriented 70° from the radial plane; □, off centreline, $r/x = 0.15$, 0° orientation; ○, off centreline, $r/x = 0.15$, 70° orientation (see also figure 20 for probe position and table 2 for flow conditions). All measurements were in heated jets.

from the radial direction in the plane containing the radius and centreline. Ideally we would have liked to measure the difference at 90° from the radial direction, i.e. in the x-direction, but probe interference precludes this. The 70° compromise was chosen because this was the largest angle that could be used without noticeable probe interference.

In figure 18 we have plotted the data from table 2 of the skewness and kurtosis of the temperature difference measurements, for various probe orientations and positions, as a function of Reynolds number. The skewness data appear to show a slight upward trend with Reynolds number although the range is limited and the trend may be due to scatter. Their average value of around -0.8 is consistent with numerous other measurements in shear flows (Sreenivasan 1991). Recently it has been shown (Holzer & Siggia 1994; Tong & Warhaft 1994*b*) that even in grid-generated turbulence, where there is no shear or apparent large-scale structure, the skewness is also of order one and constant (over a grid mesh Reynolds number varying from 5×10^3 to 57×10^3). Thus the derivative skewness is a basic characteristic of all turbulent flows, not confined to those with shear and coherent structures. Notice that the kurtosis (figure 18) shows the expected increase with Reynolds number as the small-scale internal intermittency increases.

In figure 19(*a*) we have plotted the cross-correlation between the square of the signal, θ^2, and the square of the temperature difference, $(\Delta\theta)^2$, the latter being proportional to the components of the scalar dissipation, $\kappa\langle(\partial\theta/\partial x_i)(\partial\theta/\partial x_i)\rangle$. This correlation, $\rho_{\theta^2,(\Delta\theta)^2}$, is small for centreline values, but becomes significant for the off-centreline position ($r/x = 0.15$), and particularly for the temperature difference measured at 70° to the radial direction. There is a definite downward trend with Re_j, as would be expected, since as the Reynolds number increases so does the separation of scales. Thus small and large scales should become less correlated. A log-log plot of the data (not shown) shows an approximately $Re_l^{-1/2}$ dependence, suggesting that the data are not inconsistent with high-Reynolds-number scaling. Similar trends are found for $\rho_{\theta,(\Delta\theta)^2}$ (table 2, not plotted). Anselmet & Antonia (1985) also measured $\rho_{\theta^2,(\Delta\theta)^2}$ in a plane jet but

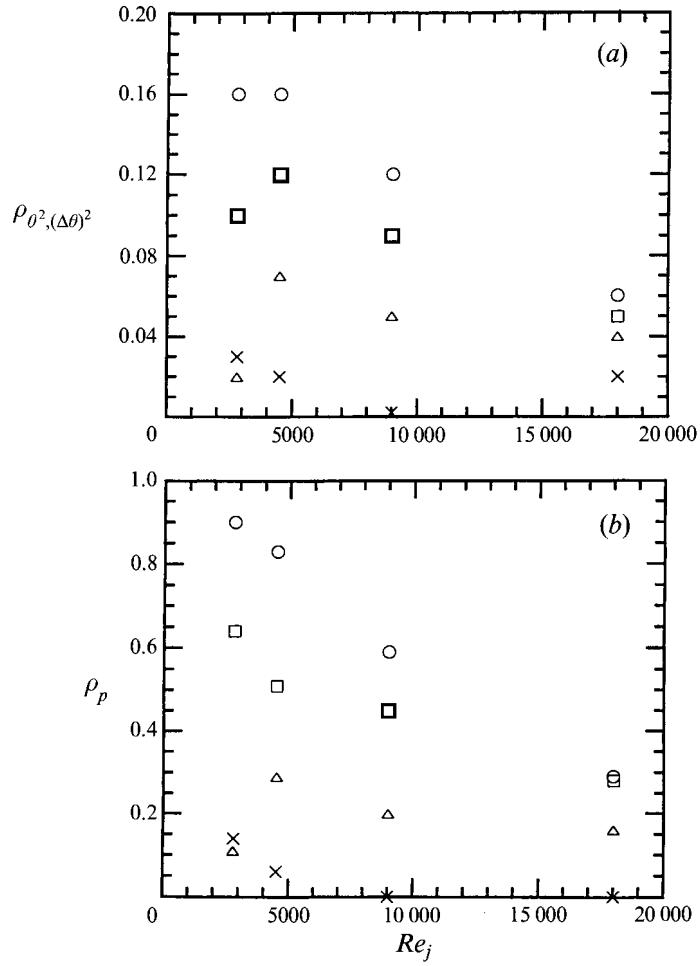

FIGURE 19. (*a*) The correlation coefficient between the square of the temperature fluctuations, θ^2, and the square of the temperature difference, $(\Delta\theta)^2$. (*b*) The correlation function $\rho_p \equiv \langle\theta^2(\Delta\theta)^2\rangle/(\langle\theta^2\rangle\langle(\Delta\theta)^2\rangle)-1$. The symbols and flow conditions are the same as in figure 18.

for one Reynolds number only ($R_\lambda = 160$), and obtained a value similar to our results. On the other hand, Djeridi (1992) found a value of 0.5 in their round jet with co-flow. The reason for this discrepancy is unclear. Another measure of the correlation between the large- and small-scale temperature fluctuations, defined as $\rho_p \equiv \langle\theta^2\epsilon_\theta\rangle/(\langle\theta^2\rangle\langle\epsilon_\theta\rangle)-1$ was used by Eswaran & Pope (1988), and this is plotted in figure 19(*b*). This is not strictly a correlation coefficient but if θ^2 and ϵ_θ are independent, ρ_p is zero. The trend of ρ_p is similar to that of $\rho_{\theta^2,(\Delta\theta)^2}$, but the magnitude is larger. Here the downward trend with Re_j is evident even for the values measured along the jet centreline. The results of figure 19 suggest that $\rho_{\theta^2,(\Delta\theta)^2}$ and ρ_p tend to zero asymptotically as Re_j becomes large. Conventional Kolmogorov theory would also indicate this. We note, however, because of the presence of the ramp–cliff structures (and hence the non-zero derivative skewness), that even at very high Re there may still be a slight residual correlation between the large and small scales, particularly off the jet centreline.

We now present some conditional statistics of the scalar as well as the velocity field. First we discuss the expectation of the scalar dissipation rate conditioned on the scalar

fluctuations, $\chi_{\epsilon_\theta} = \langle(\partial\theta/\partial x_i)(\partial\theta/\partial x_i)|\theta\rangle$. This is a quantity of interest because it is a crucial term to be modelled in the one-point scalar p.d.f. evolution equation. The general equation for the p.d.f. of scalar fluctuations, θ, is given by Sahay & O'Brien (1993):

$$\frac{\partial P}{\partial t} + \boldsymbol{U}\cdot\boldsymbol{\nabla}P + \boldsymbol{\nabla}\cdot(\mathscr{F}P) - \frac{\partial}{\partial\hat{\theta}}[\mathscr{F}\cdot\boldsymbol{\nabla}\Theta)\,P] = \kappa\nabla^2 P - \kappa\frac{\partial^2(\chi_{\epsilon_\theta}P)}{\partial\hat{\theta}^2} - \frac{\partial}{\partial\hat{\theta}}\left[\left(\frac{\partial\Theta}{\partial t} + \boldsymbol{U}\cdot\boldsymbol{\nabla}\Theta - D\nabla^2\Theta\right)P\right]. \quad (2)$$

Here $P\ (\hat{\theta};\boldsymbol{x},t)$ is the one-point p.d.f. of the scalar fluctuation, $\chi_{\epsilon_\theta}(\theta;\boldsymbol{x},t)$ and $\mathscr{F}(\theta;\boldsymbol{x},t)$ are the expectation of the square of the scalar gradient and the fluctuating velocity conditioned on scalar fluctuations respectively, $\boldsymbol{U}(\boldsymbol{x},t)$ and $\Theta(\boldsymbol{x},t)$ are mean velocity and mean scalar fields. The term containing χ_{ϵ_θ} represents molecular diffusion in θ-space, which is key to the evolution of the scalar p.d.f. For the case of a homogeneous velocity and scalar field it is the only unclosed term (Eswaran & Pope 1988). Also, χ_{ϵ_θ} indicates the level of the correlation between the scalar fluctuations and its dissipation. It can be shown that the independence of χ_{ϵ_θ} of the magnitude of scalar fluctuations is a necessary and sufficient condition for the scalar p.d.f. to be Gaussian (Pope 1985; O'Brien 1991). Moreover, χ_{ϵ_θ} is an important quantity in the analysis of turbulent diffusion flames. In the case of a one-step irreversible fast-chemistry reaction, the mean reaction (chemical production) rate is proportional to the expectation of the scalar dissipation conditioned on the stoichiometric mixture fraction (Bilger 1989).

In the present experiment we determined the conditional expectation of single components of the temperature dissipation only. Thus we evaluated $\langle(\Delta\theta)^2|\theta\rangle$, where $\Delta\theta$ was determined in the radial direction and at 45° and 70° to this direction. (The measurements in the azimuthal direction were done at one location, $r/x = 0.15$, where r is the distance from the jet centreline.) The results of these one-component conditional scalar dissipation measurements normalized by $\langle(\Delta\theta)^2\rangle$ are shown in figure 20. On the jet centreline (figure 20*a*), $\langle(\Delta\theta)^2|\theta\rangle_{0°}$ is nearly independent of θ/σ_θ for $|\theta/\sigma_\theta| < 3$, where σ_θ is the r.m.s. value of θ. (The departure from unity for $|\theta/\sigma_\theta| > 3$ appears to be due to statistical uncertainty.) Here the subscript is the angle between the two temperature probes and the radial direction (see the sketches in figures). However, when the jet centreline temperature derivative was determined with a significant longitudinal component, the results show a qualitative change (figure 20*a*). Thus $\langle(\Delta\theta)^2|\theta\rangle_{70°}$ is not flat, but has large values associated with large negative temperature fluctuations. This directional dependence is probably due to rare thin and possibly sheet-like structures associated with the entrainment of the cold ambient fluid, causing sharp scalar gradients with a strong component in the streamwise direction. As the probes are moved towards the edge of the jet ($r/x = 0.11$ and 0.15), $\langle(\Delta\theta)^2|\theta\rangle_{0°}$ increases significantly with positive θ (figure 20*c*), indicating that the large positive fluctuations from the centre of the jet are associated with higher scalar dissipation. Also plotted in figure 20(*c*) is the conditional expectation at $r/x = 0.15$ for the probe separation in the azimuthal direction. Here the shape is similar to the 0° case, indicating that there is no directional dependence within the radial plane. Finally, in figure 20(*d*) we have plotted $\langle(\Delta\theta)^2|\theta\rangle_{70°}$ for the same off centreline locations as in figure 20(*c*). Here the conditional expectation becomes U-shaped as r increases. The left-hand lobe appears to be associated with the entrainment mechanism observed in

figure 20(*b*) for the same probe orientation on the jet centreline. The right-hand lobe, associated with large temperature fluctuations originating at the centreline of the jet, is similar to the lobe observed in figure 20(*c*) for the probe separation in the radial and azimuthal directions. Unlike the entrainment mechanism which appears to be highly angle dependent, the right-hand lobe is independent of probe separation direction, only depending on r, the distance from the jet centreline.

The measurements for the conditional expectation of $(\Delta\theta)^2$ were done at the highest Reynolds number ($Re_j = 18000$, $Re_l = 2600$). It is important to note that even at this high Re there is a significant dependence of $(\Delta\theta)^2$ on θ (particularly when the probe angle is 70°), even though $\rho_{\theta^2,(\Delta\theta)^2}$ is very close to zero (figure 19*a*). This shows that $\langle(\Delta\theta)^2|\theta\rangle$ is a more sensitive indicator of the dependence of the small scales on the large scales than is the cross-correlation coefficient.

Our results for the conditional expectation of $(\Delta\theta)^2$ appear to be at variance with those obtained by Kailasnath, Sreenivasan & Saylor (1993) in water jets. Their results (figure 5 of their paper) show that both $\langle(\partial c/\partial x)^2|c\rangle$ and $\langle(\partial c/\partial r)^2|c\rangle$ increase with the concentration fluctuations, c. Although the Schmidt number, Sc, in their experiments is approximately 600, they argued that their results for the high-Schmidt-number flow, if resolved only to the Kolmogorov scale, could be interpretated as having unity Sc (or Pr). This would be the case if the mixing process followed the classical cascade picture, i.e. with molecular mixing taking place at the smallest scale and its rate being independent of the value of the molecular diffusivity. However, the Schmidt number is known to influence the mixing rate in shear flows even at high Reynolds numbers (Broadwell & Breidenthal 1982; Broadwell & Mungal 1988, 1991). Broadwell & Mungal (1991) pointed out that the diffusion layer between the jet and ambient fluid, which has a thickness $\delta_d \sim l/(ScRe)^{1/2}$ (Broadwell 1989), contributes a significant amount to the mixing rate in gaseous jets, while the contribution is negligible for high-Schmidt-number flows. This is because the thickness of the diffusion layer decreases with the molecular diffusivity. Also, as discussed above, in flows with a mean scalar gradient, there exist 'ramp–cliff'-type structures in the scalar field over which there is a scalar level jump of order $\langle\theta^2\rangle^{1/2}$. Tong & Warhaft (1994*b*) have shown that the average cliff thickness, δ, is of order $(\kappa l/u)^{1/2}$. This varies with Schmidt number (for $Sc \sim 1$, δ is of the order of the Taylor microscale λ). Thus the contributions to the scalar difference at the Kolmogorov scale, from both the diffusion layers and the ramp–cliff structures, depend on the molecular diffusivity. Therefore, it is unclear how to interpret results only resolved to the Kolmogorov scale for high Schmidt-number flows.

There are some theoretical predictions of the relation between scalar p.d.f. and the conditional dissipation. Sinai & Yakhot (1989) obtained a relation for a homogeneous decaying passive scalar without a mean gradient, expressing the limiting normalized scalar p.d.f. ($t \to \infty$) in terms of χ_{ϵ_θ}:

$$P(\theta) = C\left\{\frac{\chi_{\epsilon_\theta}}{\langle\epsilon_\theta\rangle}\right\}^{-1} \exp\left\{-\int_0^\theta \frac{x\,\mathrm{d}x}{\chi_{\epsilon_\theta}(x)\langle\epsilon_\theta\rangle}\right\}. \tag{3}$$

Here θ is the normalized scalar fluctuation ($\sigma_\theta = 1$). A more general formula, relating the p.d.f. of any (normalized) stationary process, $X(t)$, and the conditional expectation of the square of its time derivative, $\langle\dot{X}^2|x\rangle$, was derived by Pope & Ching (1993):

$$P(x) = C\langle\dot{X}^2|x\rangle^{-1} \exp\left\{-\int_0^x \frac{\langle\ddot{X}|x'\rangle\,\mathrm{d}x'}{\langle\dot{X}^2|x'\rangle}\right\}. \tag{4}$$

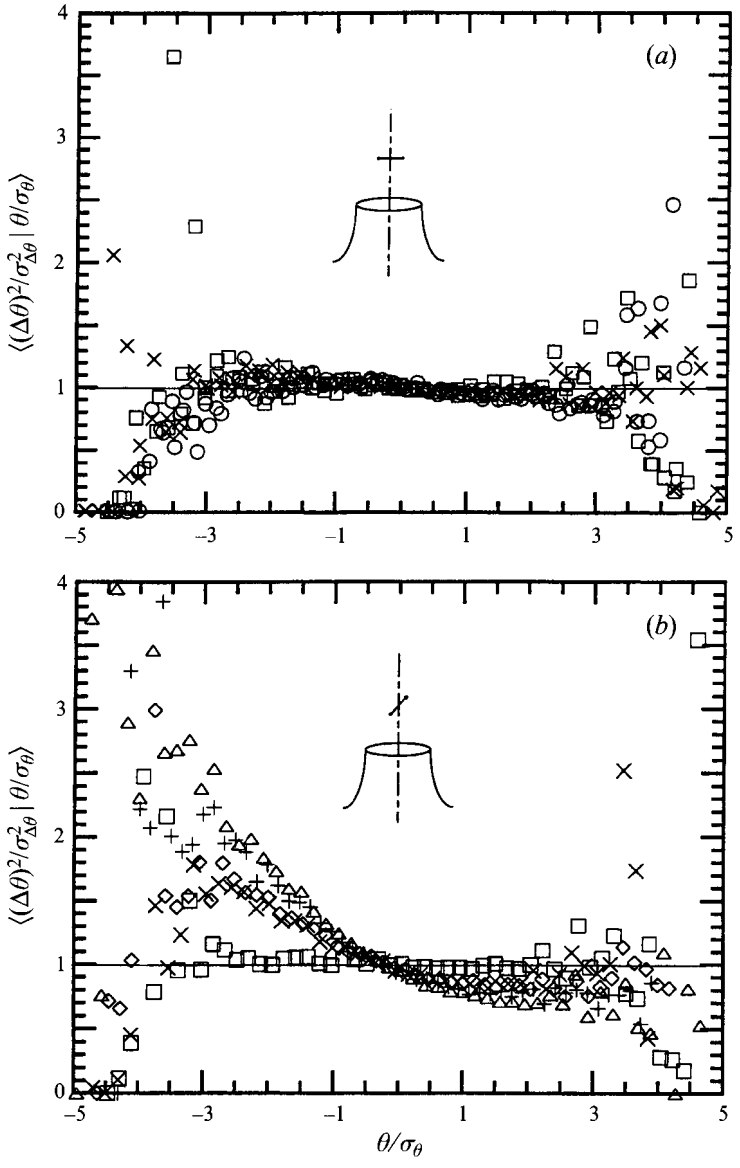

FIGURE 20(*a*, *b*). For caption see facing page.

Here the overdot indicates a time derivative. Pope & Ching (1993) pointed out that (3) and (4) are formally the same if

$$\langle \ddot{X}|x\rangle/\langle \dot{X}^2\rangle = -x. \tag{5}$$

While (5) must be valid for a decaying homogeneous isotropic scalar field (note that for a homogeneous scalar field, the time derivative can be replaced by spatial derivative), it is worthwhile asking whether (5) is valid for more general flows. If so, then (3) could be used to close the p.d.f. equation. A few recent experiments have indicated that (5) may be a good assumption even for non-Gaussian process. Thus Pope & Ching (1993) computed $\langle(\partial^2\theta/\partial t^2)\,|\,\theta\rangle/\langle(\partial\theta/\partial t)^2\rangle$ from the Chicago convection data and found good agreement with (5). Further measurements in grid turbulence with a linear temperature profile by Jayesh in our research group (private

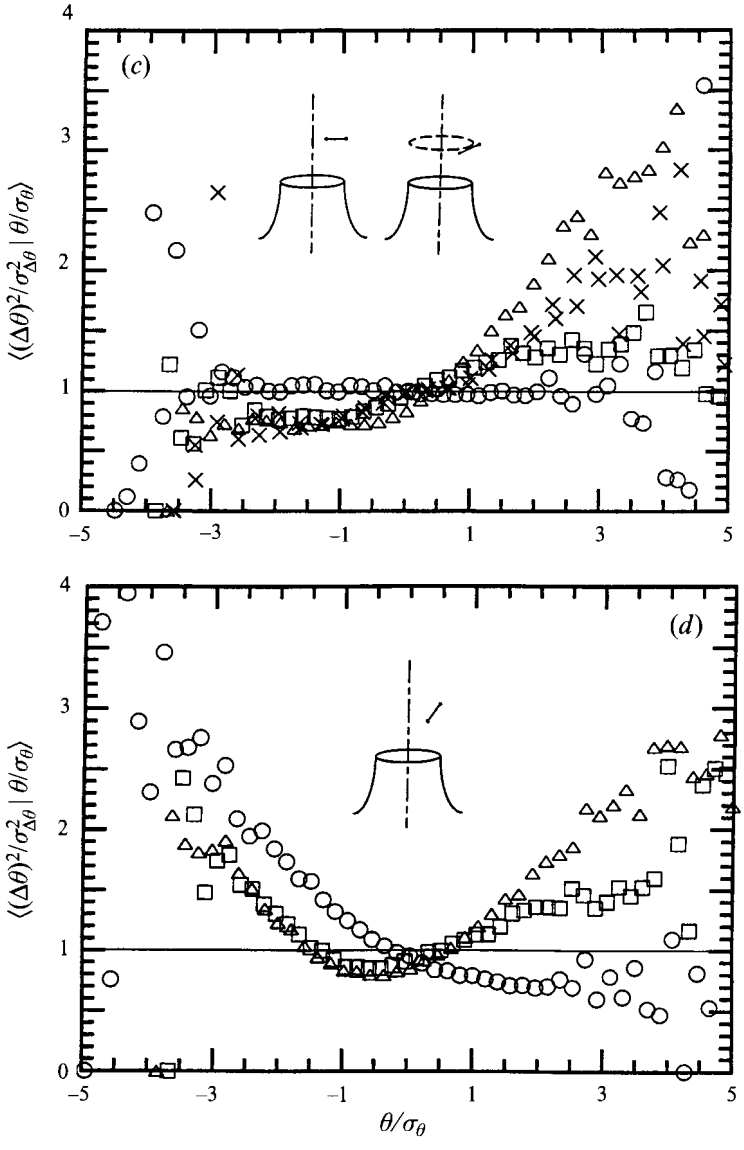

FIGURE 20. The conditional expectation of $(\Delta\theta)^2$ on θ, normalized by the variance of the difference, $\sigma^2_{\Delta\theta}$ and the r.m.s. temperature, σ_θ, respectively. The probe orientation and position is sketched on the pictures. (*a*) Measurements on the jet centreline at $x/D_j = 40$ with probe spacing in the radial plane: ○, heated jet ($D_j = 15$ mm, $U_j = 18$ m s^{-1}); ×, heated 15 mm ring placed at $x/D_j = 4$ ($D_j = 15$ mm, $U_j = 9$ m s^{-1}); □, heated 15 mm ring placed at $x/D_j = 4$ ($D_j = 15$ mm, $U_j = 18$ m s^{-1}); (*b*) Centreline measurements with the probe orientation varied. For all cases $D_j = 15$ mm, $U_j = 18$ m s^{-1} and the measurements were at $x/D_j = 40$: □, heated ring, 0° orientation; ◇, heated ring 45°; △, heated ring 70°; ×, heated jet 45°; +, heated jet 70°. The heated ring was of 15 mm diameter placed at $x/D_j = 4$. (*c*) Off centreline measurements at $x/D_j = 40$ with the probe in the radial and azimuthal directions: □, heated ring, probe at $r/x = 0.11$, 0°; △, heated ring, probe at $r/x = 0.15$, 0°; ○, heated ring, probe on the centreline (data from (*a*) for comparison); ×, heated ring, probe at $r/x = 0.15$, azimuthal direction. $D_j = 15$ mm, $U_j = 18$ m s^{-1} and the ring diameter is 15 mm, placed at $x/D_j = 4$. (*d*) heated ring (15 mm diameter placed at $x/D_j = 4$, $D_j = 15$ mm, $U_j = 18$ m s^{-1}) for a probe angle of 70° but with variation of r/x: ○, centreline (same as triangles in *b*); □, $r/x = 0.11$; △, $r/x = 0.15$. The measurement location was at $x/D_j = 40$.

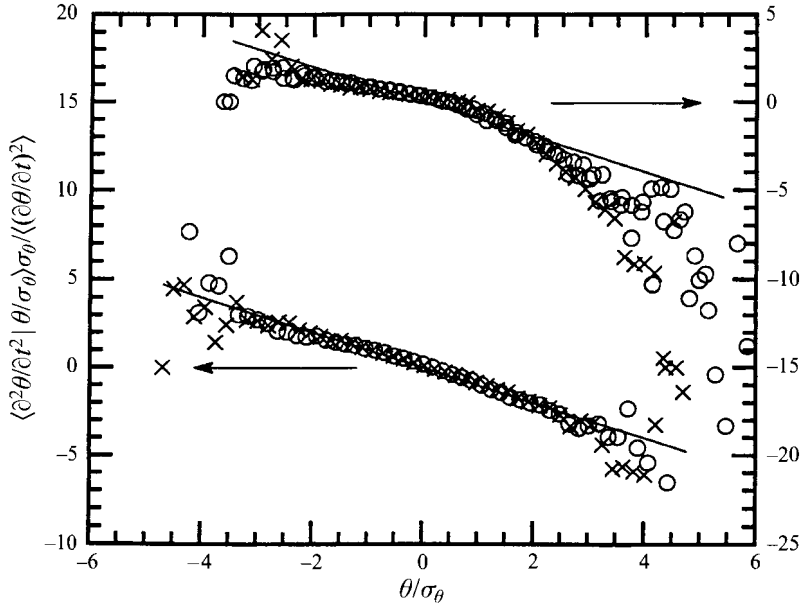

FIGURE 21. The conditional expectation of $\partial^2\theta/\partial t^2$ on θ, normalized by $\langle(\partial\theta/\partial t)^2\rangle/\sigma_\theta$ and σ_θ respectively. For both off the centreline ($r/x = 0.11$, upper curves) and on the centreline (lower), $D_j = 15$ mm and the measurements were at $x/D_j = 40$ in the heated jet. ×, $U_j = 9$ m s^{-1}; ○, $U_j = 18$ m s^{-1}.

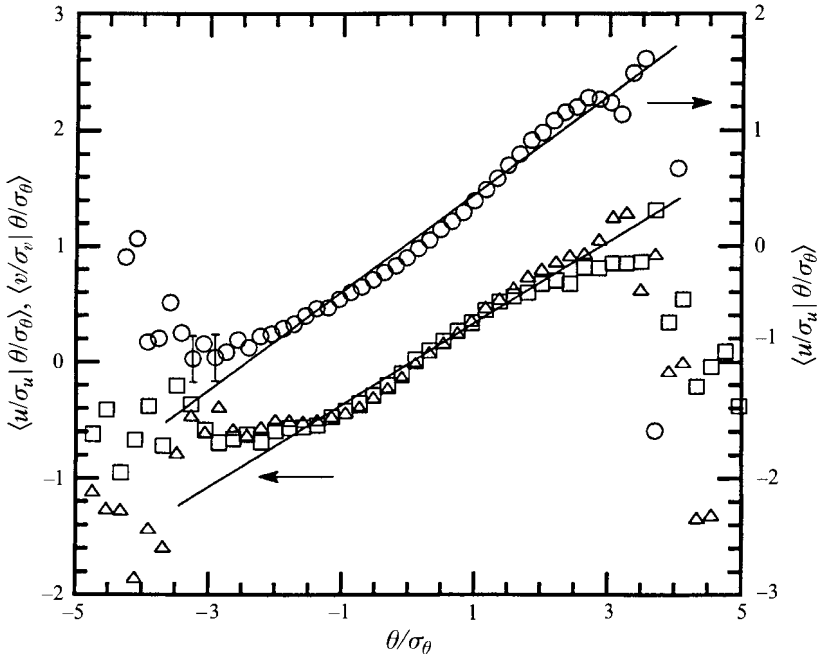

FIGURE 22. The conditional expectation of fluctuation velocity on θ, normalized by the respective r.m.s. values. $U_j = 18$ m s^{-1} and the measurements were at $x/D_j = 40$ of the heated jet. The solid lines have slopes equal to $\rho_{u,\theta}$ or $\rho_{v,\theta}$. ○, $\langle u/\sigma_u|\,\theta/\sigma_\theta\rangle$, centreline, $\rho_{u,\theta} = 0.42$; △, off centreline, $r/x = 0.05$, $\langle u/\sigma_u|\,\theta/\sigma_\theta\rangle$, $\rho_{u,\theta} = 0.37$; □, $\langle v/\sigma_v|\,\theta/\sigma_\theta\rangle$, $\rho_{v,\theta} = 0.36$, off centreline, $r/x = 0.05$.

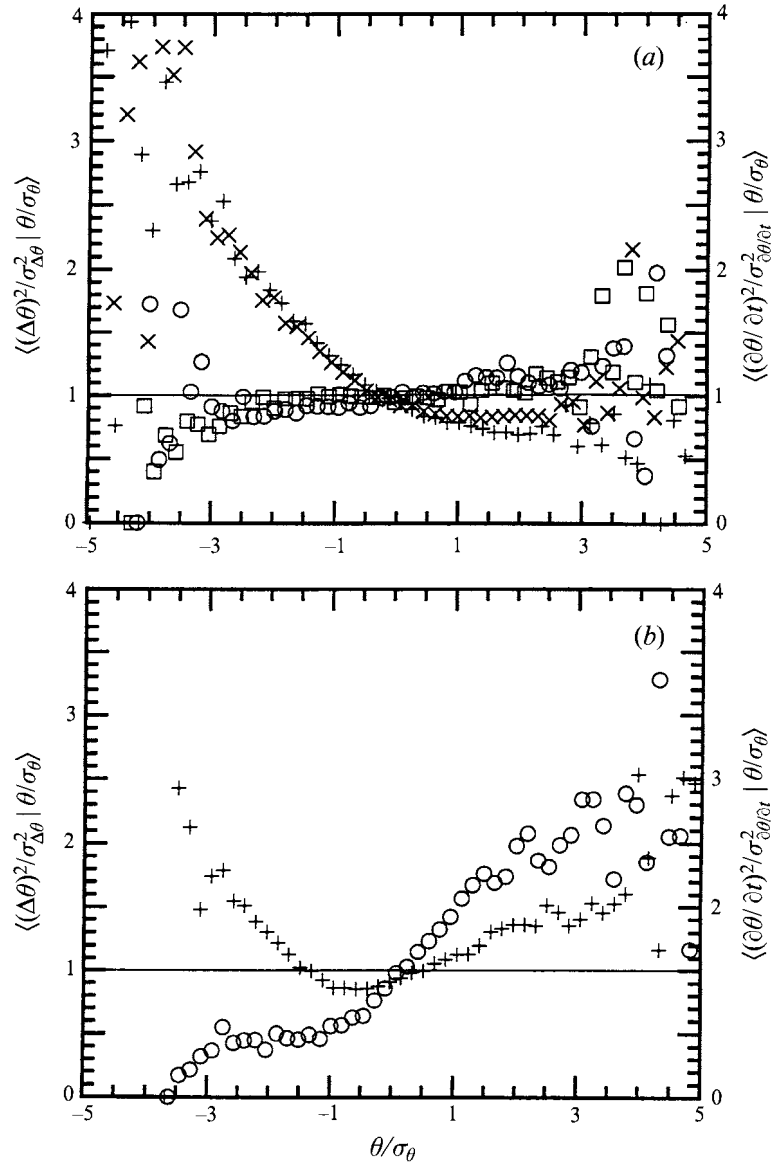

FIGURE 23. Comparison of the conditional expectation (on θ) of $(\Delta\theta)^2$ and $(\partial\theta/\partial t)^2$: (*a*) Centreline: □ ($U_j = 9$ m s^{-1}) and ○ ($U_j = 18$ m s^{-1}), $\langle(\partial\theta/\partial t)^2/\langle(\partial\theta/\partial t)^2\rangle\,|\,\theta/\sigma_\theta\rangle$ measured at $x/D_j = 40$ for the heated ring (diameter 15 mm placed at $x/D_j = 4$ with $D_j = 15$ mm); × ($U_j = 9$ m s^{-1}) and + (18 m s^{-1}), $\langle(\Delta\theta)^2/\sigma^2_{\Delta\theta}|\theta/\sigma_\theta\rangle$ for probe at 70° to radial plane, same conditions as for the time derivative measurements. (*b*) Off centreline: ○, $\langle(\partial\theta/\partial t)^2/\langle(\partial\theta/\partial t)^2\rangle\,|\,\theta/\sigma_\theta\rangle$ measured at $x/r = 0.11$, compared with $\langle(\Delta\theta)^2/\sigma^2_{\Delta\theta}|\theta/\sigma_\theta\rangle$; +, measured at the same location with a 70° probe orientation. $D_j = 15$ mm, $U_j = 18$ m s^{-1}, and the 15 mm ring was at $x/D_j = 4$.

communication) also support the validity of the relationship. However, our present work shows some departure. In figure 21 we have plotted

$$\langle(\partial^2\theta/\partial t^2)\,|\,\theta/\sigma_\theta\rangle\,\sigma_\theta/\langle(\partial\theta/\partial t)^2\rangle$$

as a function of θ/σ_θ. While the relation is linear on the jet centreline, it shows significant departure for measurements off the centreline, particularly for $\theta/\sigma_\theta > 1$.

(Here we return back to the use of θ as the un-normalized temperature fluctuations.) We conjecture that the departure is due to the large-scale intermittency in the off-centreline part of the jet, which causes the conditional expectation to become the sum of two approximately piecewise linear parts.

In the one-point scalar p.d.f. transport equation of inhomogeneous turbulent flow with mean scalar gradient (equation (2)), besides $\langle \epsilon_\theta | \theta \rangle$, there exists another unclosed term, the expectation of velocity fluctuations conditioned on temperature fluctuations, $\mathscr{F}(\hat{\theta}; \boldsymbol{x}, t)$. Sahay & O'Brien (1993) propose that this term be modelled as an odd-order polynomial for the case of isotropic turbulence with a mean temperature gradient, with the conditional p.d.f., $P(v|\theta)$, taking the joint normal form. Since for the joint normal distribution $\langle v|\theta \rangle$ is linear, the higher-order term models the deviation from the joint normal distribution. Figure 22 shows that both $\langle u|\theta \rangle$ and $\langle v|\theta \rangle$ are indeed close to the values for a joint normal distribution between velocity and temperature, except for large negative temperature fluctuations. The lines have the slope of the correlation coefficient between the fluctuation velocity components and θ. The departures of $\langle u|\theta \rangle$ and $\langle v|\theta \rangle$ from the straight line, associated with cold air, are possibly due to the contamination of the hot-wire probe caused by flow reversal.

Finally, we compare results for the conditional dissipation determined using Taylor's hypothesis to direct spatial measurement in the jet. The use of Taylor's hypothesis in high-intensity shear flows has been investigated by Lumley (1965), Wyngaard & Clifford (1977), Gibson, Friehe & McConnell (1977), Champagne (1978), Antonia, Chambers & Phan-Thien (1980), Mi & Antonia (1994) and Zaman & Hussain (1981). Kailasnath *et al.* (1993) computed the conditional expectation, $\langle (\partial c/\partial x)^2 | c \rangle$ from their data taken on the jet centreline (at $x/D_j = 37$) using Taylor's hypothesis, and also measured it directly. Their results show departures for positive concentration fluctuations. However, contrary to Kailasnath *et al.* (1993), our results (figure 23) show departures for both positive and negative fluctuations. (As noted before, the form of $\langle (\Delta\theta)^2 | \theta \rangle$ of our results is quite different to that of Kailasnath *et al.*) Both on and off the jet centreline, the conditional expectation is underestimated for negative temperature fluctuations and overestimated for positive fluctuations. This is because the cold air entrained into the jet is accompanied by low streamwise convection velocity.

4. Discussion

In the far field where the rings produce the (statistically) same scalar field as the heated jet, our results have covered a sufficiently broad Reynolds-number range to show trends in the kurtosis of the temperature difference, and in the correlation between the signal variance and its squared difference. The latter tends to zero at high Reynolds numbers (figure 19) suggesting that we have captured the salient characteristics of high-Reynolds-number mixing in a jet. On the other hand, the dispersion and mixing for the near field were studied for one Reynolds number only, $Re_j = 18000$ ($Re_l = 2300$, $R_\lambda = 190$). However here, for our dispersion experiments, we were concerned only with the turbulent convective and diffusive range and not the predominantly molecular spreading range that occurs very close to the sources (Warhaft 1984). For these ranges the spreading of the scalar does not depend on thermal diffusitivity. (The molecular diffusive range was not studied here because the size of the wire used for the ring and point sources was larger than the molecular diffusive range.) For the case of the mixing of two scalars, the situation is slightly more complicated since molecular diffusion is necessary to produce positive ρ. The time

needed for the mixing to reach the molecular level is similar to that for any quantity to be transferred from the integral to dissipation scales. Lumley (1992) estimates it as $2l/u(1-1.29Re_l^{-1/2})$, using the spectral transfer model suggested by Tennekes & Lumley (1972). It approaches $2l/u$, twice the value of the integral timescale of the flow, as $Re_l \to \infty$. Thus for $Re_l = 2300$ the second term in the Lumley expression is small, and we expect the rate of molecular mixing of the two scalars, as well as the evolution of ρ and $\rho(f)$, to be independent of the Reynolds number.

The directional dependence of $\langle(\Delta\theta)^2|\theta\rangle$ (figure 20) indicates anisotropy of the small scales of the thermal field at second moment level. A commonly used parameter to measure the anisotropy at this level is the ratio of the variance of the derivative in two directions, e.g. $\langle(\partial\theta/\partial r)^2\rangle/\langle(\partial\theta/\partial x)^2\rangle$. Antonia, Anselmet & Chambers (1986*a*) obtained a value of 2 for this ratio on the centreline of a plane jet. In the round jet experiment, Antonia & Mi (1993) found the ratio was close to 1 and concluded that local isotropy was a better approximation for a round jet than for a plane jet. We too find that the derivative variance ratio is close to 1 (measured on the jet centreline at $x/D_j = 40$ for $Re_j = 18000$). Our results (table 2) show, on the other hand, that the skewness of the streamwise temperature derivative, which indicates anisotropy at third moment level, is approximately the same for both cases: -0.9 for the round jet in the present experiment compared with -0.85 for the plane jet (Antonia *et al.* 1986*a*). Thus the third moments appear to be more sensitive indicators of anisotropy than the second moments. The contribution to the scalar derivative variance from the ramp–cliff structures, which makes up the difference between $\langle(\partial\theta/\partial r)^2\rangle$ and $\langle(\partial\theta/\partial x)^2\rangle$, comes from scales larger than those that contribute most to the skewness. Therefore the variance ratio tends to be influenced more by large-scale motions. This may explain the large variation of $\langle(\partial\theta/\partial r)^2\rangle/\langle(\partial\theta/\partial x)\rangle^2$ for different flows with similar value of skewness. Compared to the complex coherent structures of a round jet, which is dominated by axisymmetric and helical modes (Broadwell & Mungal 1991), the structures of a plane jet are relatively simple. Here the vortical structures are primarily aligned in the spanwise direction (Antonia *et al.* 1986*b*; Tso & Hussain 1989) and tend to produce temperature structures in certain directions, and thus the derivative ratio is higher. We note that the variance ratio measures the directional dependence of the temperature derivative (rotation) whereas $S_{\theta x}$ (the derivative skewness in the mean flow direction) reveals asymmetry in one direction (reflection).

The anisotropy and non-zero skewness of the temperature derivative in the shear flows has been studied by a number of workers (Mestayer *et al.* 1976; Gibson *et al.* 1977; Sreenivasan *et al.* 1979; Tavoularis & Corrsin 1981; Mestayer 1982; Antonia *et al.* 1986*a*, *b*). It has generally been accepted that the ramp–cliff-type temperature structures observed in such flows, caused by large-scale coherent structures in the velocity field, are responsible for the anisotropy and skewness. However non-zero skewness was also observed in isotropic grid turbulence with mean temperature gradients (Budwig, Tavoularis & Corrsin 1985; Thoroddsen & Van Atta 1993; Tong & Warhaft 1994*b*) and in the DNS of stationary isotropic turbulence with a linear scalar profile (Pumir 1994). Tong & Warhaft (1994*b*) showed that ramp–cliff structures exist in grid turbulence over a wide Reynolds-number range. They found $\langle(\partial\theta/\partial y)^2\rangle/\langle(\partial\theta/\partial x)\rangle^2 = 1.5$ and $S_{\theta y}$ (the derivative skewness along the mean gradient) $= 1.8$. Here y is the direction of mean gradient. They also showed, as mentioned above, that although the mean thickness of these cliffs scaled with Taylor microscale λ, the contribution to the skewness mainly came from much smaller scales, i.e. thinner structures which are possibly embedded in the large structures. Thus the non-zero skewness does not depend on any specific type of large-scale structure and is

inherent to all turbulent flows. It is even observed in two-dimensional simulations of a linear mean scalar profile in isotropic turbulence (Holzer & Siggia 1994).

5. Conclusions

Our experimental study has focused on two broad aspects of passive scalar behaviour in a turbulent jet. First, by introducing two scalar fields independently of each other, we have observed how they spread from their sources and then mix with each other within the jet. An understanding of the mixing of two scalars separated by a surrounding medium is very important in atmospheric pollution problems as well as in laboratory and industrial mixers. Here the dispersion is intimately related to the mixing rate. The second aspect of the experiment has been concerned with the scalar concentration in the jet farther downstream, where the two sources have completely mixed with each other. Here we have shown that the scalar field is independent of how it is introduced (be it from heated rings or from heating the whole jet). The scalar fluctuations are now completely determined by the mixing of the warm jet with its surroundings. In this region, which we have called the far field, the temperature field is self-similar. We will now summarize our main findings.

The scalar field from a single heated ring (§3.2) produces very large fluctuations close to the source, but after about 1.5 eddy turnover times (at $x/D_j \approx 20$ if the ring was placed at $x/D_j = 9$, figure 5), the fluctuating scalar field becomes similar to that produced by traditional heated jets. Dispersion from a very small ring (approximating a point source) produced mean profiles that are Gaussian in both the near and far field (figure 7), while for the larger rings the mean profiles were a function of the ring diameter in the near field (figure 6*a*), only becoming Gaussian in the far field. The evolution of the half-width of the point source profile showed two ranges: an initial approximately linear growth followed by a slower growth rate, consistent with $x^{1/2}$ (figure 8). For all the heated ring experiments the asymptotic value of the scalar fluctuation intensity, $\langle\theta^2\rangle^{1/2}/T_c$, is approximately 0.2, the same as that observed in heated jet experiments.

When two heated rings were used to study the mixing of two independently introduced scalar fields (§3.3), we have shown that the cross-correlation coefficient, ρ, between the two scalars is initially dependent on the ring configurations, having either positive or negative values close to the rings (figure 9). However by about 1.5 eddy turnover times, ρ tends to unity irrespective of initial conditions (figures 9 and 14). This rapid mixing is contrasted with that of two-scalar mixing in grid turbulence where complete mixing takes 3–4 eddy turnover times (figure 9). The early evolution of the segregation parameter, α, is also strongly dependent on initial conditions, but for the jet it approaches its asymptotic value of 0.04 in 1.5 eddy turnover times (figure 11*a*), while in grid turbulence it takes over 4 eddy turnover times to reach its (apparent) asymptotic value of around 0.2 (figure 11*b*). Our results on the coherence (figure 13) show that the large scales tend to lead the small scales in their evolution.

In the far field, where $\rho = 1$ (§3.4), our measurements were done using either a heated jet or heated rings, since here the thermal field is the same regardless of its origin. Here the scalar p.d.f.'s are Gaussian along the jet centreline (figure 15) but significantly skewed to the high-temperature fluctuations off the jet centreline (figure 16). The scalar spectrum (along the centreline) shows a scaling region of slope 1.37, while that of the velocity is 1.47 (figure 17). Measurements of the scalar derivative kurtosis (figure 18) show the expected upward trend with (jet) Reynolds number, which was varied from 4500 to 18000.

Considerable attention was given to the relationship between the integral-scale scalar fluctuations, and the dissipation-scale fluctuations, in the far field. The correlation between θ^2 and $(\Delta\theta)^2$ showed a significant downward trend with Re_j (figure 19), decreasing as approximately $Re_l^{-1/2}$. This could be expected since the large and small scales become less coupled as Re increase. On the other hand the conditional expectation of $(\Delta\theta)^2$ on θ, determined for temperature differences measured at various angles to the flow, showed that $(\Delta\theta)^2$ is still significantly dependent on θ even at the highest Reynolds number we have studied (figure 20). We have noted that the conditional scalar dissipation is a significant term in the scalar p.d.f. equation. We showed that another term in the p.d.f. equation, the conditional expectation of the velocity fluctuations on θ, is close to the joint normal values (figure 22). We also investigated the expectation of $\partial^2\theta/\partial t^2$ conditioned on θ and showed that is a nonlinear function of θ off the jet centreline (figure 21). Finally we have shown that Taylor's hypothesis, when used for determining conditional statistics, fails both on and off the jet centreline (figure 23).

We thank Professor John Lumley for the use of the jet facility and Mr Edward Jordan for his continued help with the technical aspects. This work was funded by the Department of Energy, Basic Energy Science. We thank them for their support.

REFERENCES

ANAND, M. S. & POPE, S. B. 1985 Diffusion behind a line source in grid turbulence. In *Proc. 4th Symp. on Turbulent Shear Flows,* pp. 46–61. Springer.

ANSELMET, F. & ANTONIA, R. A. 1985 Joint Statistics between temperature and its dissipation in a turbulent jet. *Phys. Fluids* **28**, 1048–1054.

ANTONIA, R. A., ANSELMET, F. & CHAMBERS, A. J. 1986*a* Assessment of local isotropy using measurements in a turbulent plane jet. *J. Fluid Mech.* **163**, 365–391.

ANTONIA, R. A., CHAMBERS, A. J., BRITZ, D. & BROWNE, L. W. B. 1986*b* Organized structures in a turbulent plane jet: topology and contribution to momentum and heat transport. *J. Fluid Mech.* **172**, 211–229.

ANTONIA, R. A., CHAMBERS, A. J. & PHAN-THIEN, N. 1980 Taylor's hypothesis and spectra of velocity and temperature derivatives in a turbulent shear layer. *Boundary-Layer Met.* **19**, 19–29.

ANTONIA, R. A. & MI, J. 1993 Temperature dissipation in a turbulent round jet. *J. Fluid Mech.* **250**, 531–551.

BATCHELOR, G. K. 1952 Diffusion in a field of homogeneous turbulence II. The relative motion of particles. *Proc. Camb. Phil. Soc.* **48**, 345–362.

BENNANI, A., GENCE, J. N. & MATHIEU, J. 1985 The influence of a grid-generated turbulence on the development of chemical reactions. *AIChE J.* **31**, 1157–1166.

BILGER, R. W. 1989 Turbulent diffusion flames. *Ann. Rev. Fluid Mech.* **21**, 101–135.

BILGER, R. W., MUDFORD, N. R. & ATKINSON, J. D. 1985 Comments on 'Turbulent effects on the chemical reaction for a jet in a nonturbulent stream and for a plume in a grid-generated turbulence'. *Phys. Fluids* **28**, 3175–3177.

BREIDENTHAL, R. E. 1981 Structure in turbulent mixing layers and wakes using a chemical reaction. *J. Fluid Mech.* **109**, 1–24.

BROADWELL, J. E. 1989 A model for reactions in turbulent jets: effects of Reynolds, Schmidt, and Damköhler numbers. In *Turbulent Reactive Flows*, Lecture Notes in Engineering. vol. 40, pp. 257–277. Springer.

BROADWELL, J. E. & BREIDENTHAL, R. E. 1982 A simple model of mixing and chemical reaction in a turbulent shear layer. *J. Fluid Mech.* **125**, 397–410.

BROADWELL, J. E. & MUNGAL, M. G. 1988 Molecular mixing and chemical reactions in turbulent shear layers. In *22nd (Intl) Symp. on Combustion*, pp. 579–587. The Combustion Institute.

BROADWELL, J. E. & MUNGAL, M. G. 1991 Large-scale structures and molecular mixing. *Phys. Fluids* A **3**, 1193–1206.

BROWNE, L. W. B., ANTONIA, R. A. & CHUA, L. P. 1989 Calibration of X-probes for turbulent flow measurements. *Exps. Fluids* **7**, 201–208.

BUDWIG, R., TAVOULARIS, S. & CORRSIN, S. 1985 Temperature fluctuations and heat flux in grid-generated isotropic turbulence with streamwise and transverse mean-temperature gradients. *J. Fluid Mech.* **153**, 441–460.

CHAMPAGNE, F. H. 1978 The fine-scale structure of the turbulent velocity field. *J. Fluid Mech.* **86**, 67–108.

CHEN, C. J. & RODI, W. 1980 *Vertical Turbulent Buoyant Jets – A Review of Experimental Data.* Pergamon.

DAHM, W. J. A. & DIMOTAKIS, P. E. 1987 Measurements of entrainment and mixing in turbulent jets. *AIAA J.* **25**, 1216–1223.

DANCKWERTS, P. V. 1952 The definition and measurement of some characteristics of mixtures. *Appl. Sci. Res.* A**3**, 279–296.

DJERIDI, H. 1992 Etude de la liaison entre un scalaire passif et sa dissipation en écoulements turbulents libre et de paroi. PhD thesis, Université d'Aix-Marseille II.

DOWLING, D. R. & DIMOTAKIS, P. E. 1990 Similarity of the concentration field of gas-phase turbulent jets. *J. Fluid Mech.* **218**, 109–141.

DURBIN, P. A. 1980 A stochastic model of two particle dispersion and concentration fluctuations in homogenous turbulence. *J. Fluid Mech.* **100**, 279–302.

ESWARAN, V. & POPE, S. B. 1988 Direct numerical simulations of the turbulent mixing of a passive scalar. *Phys. Fluids* **31**, 506–520.

FACKRELL, J. E. & ROBINS, A. G. 1982 Concentration fluctuations and fluxes in plumes from point sources in a turbulent boundary layer. *J. Fluid Mech.* **117**, 1–26.

GIBSON, C. H., FRIEHE, C. A. & MCCONNELL, S. O. 1977 Structure of sheared turbulent fields. *Phys. Fluids* **20**, S156–167.

GIBSON, M. M. 1962 Spectra of turbulence in a round jet. *J. Fluid Mech.* **15**, 161–173.

HOLZER, M. & SIGGIA, E. D. 1994 Turbulent mixing of a passive scalar. *Phys. Fluids* **6**, 1820–1837.

HUNT, J. C. R. 1985 Turbulent diffusion from sources in complex flows. *Ann. Rev. Fluid Mech.* **17**, 447–485.

HUSSEIN, J. H., CAPP, S. P. & GEORGE, W. K. 1994 Velocity measurements in a high-Reynolds-number momentum-conserving, axisymmetric, turbulent jet. *J. Fluid Mech.* **258**, 31–75.

KAILASNATH, P., SREENIVASAN, K. R. & SAYLOR, J. R. 1993 Conditional scalar dissipation rates in turbulent wakes, jets, and boundary layers. *Phys. Fluids* A **5**, 3207–3215.

KARNIK, U. & TAVOULARIS, S. 1989 Measurements of heat diffusion from a continuous line source in a uniformly sheared turbulent flow. *J. Fluid Mech.* **202**, 233–261.

KERSTEIN, A. R. 1992 Linear-eddy modelling of turbulent transport. Part 7. Finite-rate chemistry and multi-stream mixing. *J. Fluid Mech.* **240**, 289–313.

KERSTEIN, A. R. & SCHEFER, R. W. 1994 A conditional similarity concept for turbulent shear flow, with application to mixing in a round jet. *Phys. Fluids* **6**, 642–651.

KOMORI, S., HUNT, J. C. R., KANZAKI, T. & MURAKAMI, Y. 1991 The effects of turbulent mixing on the correlation between two species and on concentration fluctuations in non-premixed reacting flows. *J. Fluid Mech.* **228**, 629–659.

KOMORI, S., UEDA, H. & TSUKUSHI, F. 1985 Turbulent effects on the chemical reaction in the atmosphere surface layer. In *Proc. 50th ann. meeting of the Japanese Chemical Engineers*, p. 241 (in Japanese).

LOCKWOOD, C. & MONEIB, H. A. 1980 Fluctuating temperature measurements in a heated round free jet. *Combust. Sci. Technol.* **22**, 63–81.

LUMLEY, J. L. 1965 Interpretation of time spectra measured in high-intensity shear flows. *Phys. Fluids* **8**, 1056–1062.

LUMLEY, J. L. 1992 Some comments on turbulence. *Phys. Fluids* A, 203–211.

MESTAYER, P. 1982 Local isotropy and anisotropy in a high-Reynolds-number turbulent boundary layer. *J. Fluid Mech.* **125**, 475–503.

MESTAYER, P. G., GIBSION, G. H., COANTIC, M. F. & PATEL, A. S. 1976 Local anisotropy in heated and cooled turbulent boundary layers. *Phys. Fluids* **19**, 1279–1287.

MI, J. & ANTONIA, R. A. 1994 Corrections to Taylor's hypothesis in a turbulent circular jet. *Phys. Fluids* **6**, 1548–1552.

MUDFORD, N. R. & BILGER, R. W. 1984 Examination of closure models for mean chemical reaction rate using experimental results for an isothermal turbulent reacting flow. In *Twentieth Symposium on Combustion*, pp. 387–394. The Combustion Institute.

NAKAMURA, I., SAKAI, Y. & MIYATA, M. 1987 Diffusion of matter by a non-buoyant plume in grid-generated turbulence. *J. Fluid Mech.* **178**, 379–403.

O'BRIEN, E. E. 1991 The conditional dissipation rate of an initially binary scalar in homogenous turbulence. *Phys. Fluids* A **3**, 3121–3123.

PANCHAPAKESAN, N. R. & LUMLEY, J. L. 1993 Turbulence measurements in axisymmetric jets of air and helium. Part 1. Air jet. *J. Fluid Mech.* **246**, 197–223.

PARANTHOEN, P., FOUARI, A., DUPONT, A. & LECORDIER, J. C. 1988 Dispersion measurements in turbulent flows (boundary layer and plane jet). *Intl J. Heat Mass Transfer* **31**, 153–165.

POPE, S. B. 1985 Pdf methods for turbulent reactive flows. *Prog. Energy Combust. Sci.* **11**, 119–192.

POPE, S. B. & CHING, E. S. C. 1993 Stationary probability density functions in turbulence *Phys. Fluids* **5**, 1529–1531.

PUMIR, A. 1994 A numerical study of the mixing of a passive scalar in three dimensions in the presence of a mean gradient. *Phys. Fluids* **6**, 2118–2132.

SAHAY, A. & O'BRIEN, E. 1993 Uniform mean scalar gradient in grid turbulence: Conditioned dissipation and production. *Phys. Fluids* A **5**, 1076–1078.

SCHEFER, R. W., KERSTEIN, A. R., NAMAZIAN, M. & KELLY, J. 1994 Role of large-scale structure in a nonreacting turbulent CH_4 jet. *Phys. Fluids* **6**, 652–661.

SINAI, Y. G. & YAKHOT, V. 1989 Limiting probability distributions of a passive scalar in a random velocity field. *Phys. Rev. Lett.* **63**, 1962–1964.

SIRIVAT, A. & WARHAFT, Z. 1982 The mixing of passive helium and temperature fluctuations in grid turbulence. *J. Fluid Mech.* **120**, 323–346.

SREENIVASAN, K. R. 1991 On local isotropy of passive scalars in turbulent shear flows. *Proc. R. Soc. Lond* A **434**, 165–182.

SREENIVASAN, K. R., ANTONIA, R. A. & BRITZ, D. 1979 Local isotropy and large structures in a heated turbulent jet. *J. Fluid Mech.* **94**, 745–775.

STAPOUNTZIS, H. & BRITTER, R. E. 1989 Turbulent diffusion behind a heated line source in a nearly homogenous turbulent shear flow. In *Turbulent Shear Flows* (ed. J. C. Andre *et al.*) 6, pp. 97–108. Springer.

STAPOUNTZIS, H., SAWFORD, B. L., HUNT, J. C. R. & BRITTER, R. E. 1986 Structure of temperature field downwind of a line source in grid turbulence. *J. Fluid Mech.* **165**, 401–424.

TAVOULARIS, S. & CORRSIN, S. 1981 Experiments in nearly homogeneous turbulent shear flow with a uniform mean temperature gradient. Part 2. *J. Fluid Mech.* **104**, 349–367.

TAYLOR, G. I. 1921 Diffusion by continuous movements. *Proc. Lond. Math. Soc.* A **20**, 1906–211.

TENNEKES, H. & LUMLEY, J. L. 1972 *A First Course in Turbulence.* MIT Press.

THORODDSEN, S. T. & VAN ATTA, C. W. 1992 Exponential tails and skewness of density-gradient probability density functions in stably stratified turbulence. *J. Fluid Mech.* **244**, 547–566.

TONG, C. & WARHAFT, Z. 1994*a* Turbulence suppression in a jet by means of a fine ring. *Phys. Fluids* **6**, 328–333.

TONG, C. & WARHAFT, Z. 1994*b* On passive scalar derivative statistics in grid turbulence. *Phys. Fluids* **6**, 2165–2176.

TOWNSEND, A. A. 1954 The diffusion behind a line source in homogenous turbulence. *Proc. R. Soc. Lond* A **224**, 487–512.

TSO, J. & HUSSAIN, F. 1989 Organized motions in a fully developed axisymmetric jet. *J. Fluid Mech.* **203**, 425–448.

UBEROI, M. S. & CORRSIN, S. 1953 Diffusion of heat from a line source in isotropic turbulence. *NACA Rep.* 1142.

UBEROI, M. S. & SINGH, P. I. 1975 Turbulent mixing in a two-dimensional jet. *Phys. Fluids* **18**, 764–769.

VEERAVALLI, S. & WARHAFT, Z. 1990 Thermal dispersion from a line source in the shearless turbulence mixing layer. *J. Fluid Mech.* **216**, 35–70.

VENKATARAMANI, K. S., TUTU, N. K. & CHEVRAY, R. 1975 Probability distributions in a round heated jet. *Phys. Fluids* **18**, 1413–1420.

WARHAFT, Z. 1981 The use of dual heat injection to infer scalar covariance decay in grid turbulence. *J. Fluid Mech.* **104**, 93–109.

WARHAFT, Z. 1984 The interference of thermal fields from line sources in grid turbulence. *J. Fluid Mech.* **144**, 363–387.

WARHAFT, Z. 1992 Some preliminary experiments concerning thermal dispersion in a jet. In *Studies in Turbulence* (ed. T. B. Gatski, S. Sarkar & C. G. Speziale). Springer.

WYGNANSKI, I. & FIEDLER, H. 1969 Some measurements in the self-preserving jet. *J. Fluid Mech.* **38**, 577–612.

WYNGAARD, J. C. & CLIFFORD, S. F. 1977 Taylor's hypothesis and high-frequency turbulence spectra. *J. Atmos. Sci.* **34**, 922–929.

YEUNG, P. K. & POPE, S. B. 1993 Differential diffusion of passive scalars in isotropic turbulence. *Phys. Fluids* A **5**, 2467–2478.

ZAMAN, K. B. M. Q. & HUSSAIN, A. K. M. F. 1981 Taylor hypothesis and large-scale coherent structures. *J. Fluid Mech.* **112**, 379–396.